

Performance Characterizations and Usage Guidelines of Samsung CXL Memory Module Hybrid Prototype

Jianping Zeng* Shuyi Pei* Da Zhang* Yuchen Zhou† Amir Beygi* Xuebin Yao* Ramdas Kachare*
Tong Zhang* Zongwang Li* Marie Nguyen* Rekha Pitchumani* Yang Soek Ki* Changhee Jung†
*Samsung Semiconductor, USA

{jp.zeng, shuyi.pei, zhang.da, a.beygi, xuebin.yao, r.kachare,
t.zhang2, zongwang.li, marie.n, r.pitchumani, yangsoek.ki}@samsung.com

†Purdue University, USA
{zhou1166, chjung}@purdue.edu

Abstract—The growing prevalence of data-intensive workloads, such as artificial intelligence (AI), machine learning (ML), high-performance computing (HPC), in-memory databases, and real-time analytics, has exposed limitations in conventional memory technologies like DRAM. While DRAM offers low latency and high throughput, it is constrained by high costs, scalability challenges, and volatility, making it less viable for capacity-bound and persistent applications in modern datacenters.

Recently, Compute Express Link (CXL) has emerged as a promising alternative, enabling high-speed, cacheline-granular communication between CPUs and external devices. By leveraging CXL technology, NAND flash can now be used as memory expansion, offering three-fold benefits: byte-addressability, scalable capacity, and persistence at a low cost. Samsung’s CXL Memory Module Hybrid (CMM-H) is the first product to deliver these benefits through a hardware-only solution, i.e., it does not incur any OS/I/O overheads like conventional block devices. In particular, CMM-H integrates a DRAM cache with NAND flash in a single device to deliver near-DRAM latency. This paper presents the first—publicly available—study for comprehensive characterizations of an FPGA-based CMM-H prototype. Through this study, we address users’ concerns about whether a wide variety of applications can successfully run on a memory device backed by NAND flash medium. Additionally, based on these characterizations, we provide key insights into how to best take advantage of the CMM-H device.

I. INTRODUCTION

In recent years, the emergence of data-intensive workloads, e.g., artificial intelligence (AI) [136], machine learning (ML) [72], real-time analytics [102], and high-performance computing (HPC) [131], [14], has led to exponential increases in the demand for high-performance memory [43], [60], [83], [115]. These workloads need efficient memory architectures that can store enormous amounts of data with low latency and high throughput. These demands pose significant challenges in relying solely on conventional DRAM (Dynamic Random-Access Memory), which is attached to DDR slots, to expand memory capacity due to the following issues.

First, due to its inherent hardware structures, DRAM medium scalability is constrained by physical limitations, including manufacturing cost [95], leakage current [78], and

heat dissipation [44], leading to limited memory size per module. Moreover, memory controllers only support limited DDR pin counts and yield deficient memory capacity due to significant area and power overheads as well as complicated placement, routing, and packaging problems. [18], [155]. All those issues render adopting DRAM less viable or at least challenging in large-scale datacenters for the forthcoming and future capacity-bound workloads.

In response to the above issues, storage-class memory (SCM) [11] technologies, such as STT-RAM [81], [17], ReRAM [3], [16], [152], [21], [34], [19], [20], [92], [91], MeRAM [57], [74], [108], PCM [130], [113], [77], [142], and FeRAM [101], [105], [41], [127], have emerged to offer several times larger capacity than DRAM thanks to their underlying physical materials. For example, Intel Optane memory (PMEM) [63]—based on PCM—can offer 2x larger capacity than the largest DRAM DIMMs (256 GB) and is an order of magnitude larger than typical 32 GB DRAM DIMMs used in today’s datacenters [121].

Although those SCM technologies offer higher density than DRAM, their capacities and costs are still not satisfactory. This is because (1) SCM’s internal hardware structures limit rapid increase in capacity [10] and (2) SCM is typically attached to conventional DDR slots and thus faces the same scalability issue as DRAM.

Fortunately, the first issue of medium scalability can be addressed by NAND flash technology [23], [46], [49], [99], [100], [149]. It achieves high capacity through its dense yet simple cell design without requiring complex peripheral circuitry. Besides, NAND flash can store multiple bits per cell, e.g., multi-level cell (MLC) [12], triple-level cell (TLC) [103], and quad-level cell (QLC) [86], increasing storage density significantly. Moreover, NAND flash’s simple structure makes it easier than DRAM to leverage 3D die stacking [51], [8], [94] for achieving high capacity. Consequently, while typical DRAM capacities range from 4 GB to 32 GB per module (consumer-grade) and up to 1 TB in specialized server-grade DRAM configurations, NAND flash capacities range from 128

GB to 8 TB (consumer-grade) and up to 100+ TB in enterprise-grade NAND storage systems.

In addition, NAND flash consumes significantly less energy than DRAM, mitigating heat dissipation. This is because NAND flash is nonvolatile and thus retains memory data without a constant power supply. In contrast, due to continuous power draw, DRAM needs to periodically refresh its cells to maintain data, which causes considerable energy waste. More importantly, NAND flash cells store data using a floating gate or charge trap, requiring fewer active components such as capacitors and transistors compared to DRAM.

Although NAND flash technology addresses the medium scalability and heat dissipation issues of DRAM, it operates on a block basis; i.e., it is not byte-addressable, as each NAND flash access involves transferring data in chunks much larger than a single byte. To allow for byte-granular access to external devices, industry efforts have recently focused on forming a consortium to develop Compute Express Link (CXL), an open standard for high-speed interconnects that enables an efficient, cacheline-granular, and scalable way to expand memory capacity [122], [25]. Specifically, PCIe interfaces—on which CXL operates—can deliver similar bandwidth using fewer pins compared to DDR; for example, 8 PCIe 5.0 lanes offer 32 GB/s of bandwidth per direction, while DDR5-4800 requires 160 pins to achieve 38.4 GB/s [18], allowing for higher memory capacity per pin and mitigating the DDR pin scalability issue.

In particular, CXL allows CPUs to access device memory, e.g., NAND flash, in a cache-coherent manner. That is, NAND flash is now addressable by regular load/store instructions, and its data can be maintained in CPU caches, which significantly improves the performance of cache-friendly applications. This contrasts with conventional memory-mapped I/O [50], [109], [125], [22] where flash memory contents cannot be cached in CPUs. In such cases, accesses to memory regions assigned to I/O devices are non-cacheable, thus losing the opportunity to benefit from CPU caching.

Interestingly, with the help of CXL, NAND flash can now function as persistent memory. This significantly boosts the performance of persistent applications, e.g., in-memory databases [116], [98], by eliminating costly logging to external persistent devices; please refer to Section VII for more details. The takeaway is that *CXL enables an economical way to significantly expand main memory capacity from the GB level to the TB level without losing persistence guarantee [104].*

Desiring to reap the above benefits, Samsung recently released a proof-of-concept CXL-based memory expansion device, called the CXL Memory Module Hybrid (CMM-H) [61] for emerging capacity-bound applications. As shown in Figure 1, CMM-H internally employs a DRAM cache to accelerate access to the backend NAND flash. *Thanks to the high DRAM cache hit rate, as shown in Section V-C, the CMM-H device achieves DRAM-level latency and NAND-level capacity at the same time.*

Also, CMM-H offers persistence in a fully transparent

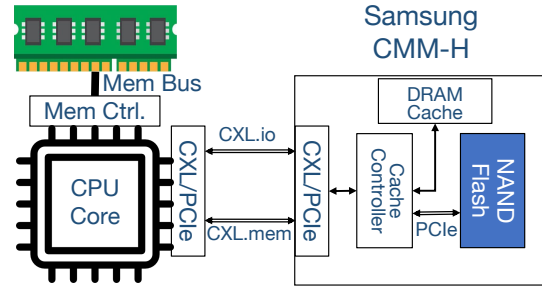


Fig. 1: High-level architecture of Samsung CMM-H; assume it is connected to conventional CPUs, though it is technically possible to attach CMM-H to other accelerators (e.g., GPUs) in the future

manner. Upon impending power loss, CMM-H flushes all volatile data in the DRAM cache to the NAND flash by using energy stored in an energy buffer (i.e., a battery), thereby transparently offering *persistence* to the upper-level software stack. Compared to conventional NVDIMMs [128] and Intel PMEM [63], CMM-H can offer a much larger memory space by exposing the high-capacity backing NAND flash to the software stack in an economical way; NVDIMMs make only DRAM space visible to software, while PMEM is still $\approx 100\times$ smaller than NAND flash.

Yet, there is no performance evaluation of CMM-H available to the public on its basic characteristics and, in particular, on how it affects persistent applications. *To bridge the gap, this paper, for the first time, conducts a comprehensive performance analysis of the CMM-H device using microbenchmarks and real-world workloads from various domains—e.g., large language models (LLMs), conventional CPU benchmark suites, high-performance computing (HPC) program, and in-memory databases—providing key insights on how to best use the CMM-H device.* In summary, this paper makes the following contributions:

- We are the first to thoroughly characterize the performance of the proof-of-concept Samsung CMM-H device, including basic read and write latencies, tail latency, and bandwidth.
- We demonstrate how the performance of the CMM-H prototype changes with varying factors, e.g., thread count, memory footprint, and program behaviors.
- We present that, with persistence ensured, CMM-H dramatically boosts the performance of persistent applications.
- With the performance analysis from the experiments, we offer key findings on how to best use the CMM-H device for both volatile and persistent applications.

II. BACKGROUND

A. Compute eXpress Link (CXL)

Compute eXpress Link (CXL) [123] is an open-standard, high-speed, and low-latency interconnect designed to enhance the performance of communication between processors, memory expanders, accelerators, and other peripherals. Built on

the PCIe physical layer, CXL extends the capabilities of traditional interconnects by offering coherence and memory-sharing features, satisfying the growing demands of modern data-intensive workloads. The upshot is that CXL’s innovative architecture enables efficient resource utilization, making it a cornerstone of next-generation computing systems [126].

For the sake of versatility and flexibility, CXL implements three protocols, `CXL.io`, `CXL.mem`, and `CXL.cache`. Among them, `CXL.io` is technically compatible with PCIe, i.e., `CXL.io` uses the same uncacheable load-store semantics for link initialization, device discovery, status reporting, virtual-to-physical address translation, and direct memory access (DMA) [25]. Owing to this guaranteed compatibility, existing PCIe devices are reusable for CXL, saving vendors’ existing considerable investments.

Meanwhile, CXL is engineered to provide nanosecond-level latency for memory accesses at cacheline granularity through `CXL.mem` protocol. That is, every access to CXL memory is byte-granular and can benefit from the cache hierarchy of the host CPUs. CXL ensures that processors can retrieve data with lower delays, significantly speeding up access to storage devices and ultimately improving computational throughput. In contrast, conventional block devices operate at page granularity (e.g., 4 KB) and thus experience significant I/O overhead—e.g., context switching, metadata maintenance, and system calls—involved in file system operations [56], due to the mismatched granularity between page and cacheline. Even though memory-mapped I/O, e.g., Linux `mmap`, can mitigate the I/O overhead, it still leads to suboptimal performance. This is because (1) uncacheable memory-mapped I/O operations [125] result in significant performance degradation for cache-friendly workloads and (2) Linux `mmap` may generate many small and random I/Os, possibly causing scalability issues [109].

In addition, with the `CXL.mem` protocol, CXL allows for memory pooling—a mechanism in which multiple processors and accelerators can dynamically access a shared pool of memory [85], [47]. This eliminates memory silos and optimizes memory utilization, enabling systems to scale efficiently without the bottlenecks of fixed memory assignments. For workloads requiring vast memory capacity, e.g., in-memory databases and real-time analytics, CXL ensures performance scalability without being limited by the finite DDR slots.

Finally, another standout feature of CXL is its support for coherent memory access via the `CXL.cache` protocol. It enables processors and devices to share data in a consistent and synchronized manner. This capability reduces the need for data duplication and movement, thus decreasing latency and conserving bandwidth. In scenarios such as GPU-accelerated computing—where accelerators rely heavily on accessing CPU memory—CXL’s coherence can provide seamless collaboration and faster execution of tasks.

B. Samsung CMM-H and Operation Modes

Recognizing CXL’s potential, Samsung took a step further by prototyping a proof-of-concept (PoC) memory expansion

device, called the CXL Memory Module Hybrid (CMM-H), which supports CXL v1.1. As depicted in Figure 1, CMM-H contains a large NAND flash, a small DRAM, and a cache controller—based on FPGA—and comes with built-in circuitry to ensure data persistence when enabled. The NAND flash offers greater capacity and lower cost than the DRAM, while the DRAM functions as a hardware-managed cache and is thus invisible to the upper-level software stack. That is, the upper-level software stack only sees the large NAND flash. Unlike conventional caches, in the version of the PoC device used in this paper, the DRAM cache¹ buffers *hot* data on a 4 KB page basis, i.e., the cache block size is 4 KB, to mitigate the long latency of accessing the NAND flash. Using page-sized blocks also simplifies communication between the DRAM cache and the NAND flash. As such, in contrast to conventional NAND flash and DRAM, this hybrid architecture enables CMM-H to achieve the following 4 goals at the same time: (1) high performance owing to DRAM cache and CXL-enabled byte addressability, (2) high capacity enabled by NAND technology, (3) low cost due to NAND flash, and (4) nonvolatility (persistence) provided by NAND flash.

CMM-H is exposed as a CPU-less NUMA node to the upper-level software stack, allowing compatibility with legacy applications. In other words, there is no need to modify existing user program as it can run directly on the platforms equipped with CMM-H. Moreover, CMM-H has the flexibility to operate either as volatile memory—i.e., dirty data in the DRAM cache is lost and the data in the NAND flash are not guaranteed to be updated (i.e., consistent) across power failures—or as persistent memory [3], [16], [52], [130], [113], [77], [119], [57], [74], [17], [80], [108]. This feature makes CMM-H a great fit for a variety of workload requirements.

1) *Device Architecture and Implementation*: In this paper, we evaluate an E3.L form-factor PoC device which is based on Versal XCV1802 FPGA². Notably, the FPGA implements a controller to manage the DRAM cache and guarantee the persistence of its data across power failures; hereafter, we refer to this controller as a DRAM cache controller for simplicity. The CMM-H device employs a PCIe Gen 4 ×4 NVMe SSD (TLC) with a capacity of 1 TB as the NAND flash portion. The device connects to the host via a PCIe Gen 4 ×8 interface and is compliant with CXL 1.1, including support for Global Persistent Flush (GPF) [25]. As a type 3 CXL device, CMM-H supports both the `CXL.io` and the `CXL.mem` protocols.

2) *Operational Behavior*: In this study, the evaluated CMM-H device is equipped with a 16 GB 8-way associative DRAM cache, which uses an LRU replacement policy and an MRU insertion policy. To quickly retrieve tags for cache accesses, an on-chip memory is dedicated to storing tags, as in prior techniques [58], [32]. However, storing tags in DRAM either incurs significant performance degradation due to doubled DRAM accesses or requires modifications on

¹We interchangeably use “DRAM cache” and “device DRAM cache” if there is no ambiguity.

²We are planning the next generation CMM-H products based on ASIC implementation to deliver lower latency and higher bandwidth.

DRAM architectures for high performance [93], [114], [55]. Because of this, the tag lookup and data probing in the DRAM cache happen sequentially.

To be specific, when the last-level cache (LLC) issues a read request (64 B granularity), the DRAM cache controller performs a tag lookup to check if the corresponding data block already resides in the DRAM cache. On a cache hit, the corresponding 64-byte data is returned immediately to the LLC. Otherwise, a 4 KB page is fetched from the NAND flash via NVMe commands and then placed into an available cache set, allowing the desired 64-byte data to be returned to the LLC later. Of course, the cache controller should first evict a cache block to the NAND flash—which is governed by LRU replacement policy—if the corresponding set in the DRAM cache is full.

Similarly, when the LLC issues a write request, the cache controller first checks whether the target data block resides in the DRAM cache by consulting the tag store. If so, the incoming data is merged into the target block, avoiding access the backing NAND flash—which is several orders of magnitude slower than DRAM—and allowing program to benefit from the fast DRAM cache. Otherwise, the controller first fetches the corresponding block from the NAND flash and then fills the block in the DRAM cache. Of course, before fetching, the DRAM cache controller evicts a block from the DRAM cache if the corresponding set in the cache is full.

3) *Persistence Support*: Beyond its use as large volatile memory, CMM-H can also function as persistent memory by enabling some specific configurations in the BIOS settings. In this mode, all (dirty) data blocks in CMM-H’s DRAM cache are ensured to be persistent across abrupt power loss, which is enabled by CXL Global Persistent Flush (GPF) [25]. That is, upon a detected power outage, the DRAM cache controller receives a signal from the host to flush the dirty blocks from the DRAM cache all the way down to the NAND flash by consuming the energy in a battery. In addition to the reactive dirty block flushing, CMM-H also supports proactive data flushing as defined by the GPF protocol. For example, upon receiving a GPF forceful flushing signal, the DRAM cache controller writes back all dirty blocks in the DRAM cache to the NAND flash, maintaining consistent memory states.

With the synergistic combination of DRAM cache and NAND flash, CMM-H achieves flexibility in operating as either volatile or persistent memory while delivering high performance and high capacity on the cheap. This enables users to optimize their applications for performance, capacity, and persistence under diverse workload scenarios. The following sections detail our experimental evaluation and analysis, highlighting the performance characteristics of the CMM-H prototype and offering guidelines for the efficient use of the CMM-H device.

C. Idempotence for Crash Consistency

Despite CMM-H’s ability to preserve data across power failures, it does not necessarily mean that program states are

automatically crash-consistent [7], [144], [71], [117], [150], [69], [141], [153], [75], [145], [143], [59], [36], [35]. For instance, as shown in Figure 2 (a), suppose a user attempts to insert an already-created new node to the beginning of a singly-linked list. This process involves two steps. First, set the `next` pointer of the new node to the address of the list’s first node `N` (①). Second, set the `next` pointer of the head node to the address of the new node (②). Now, assume a scenario, depicted in Figure 2 (b), where the second store (`str B`) has already been evicted from the LLC and thereby persists in CMM-H—assuming it operates as persistent memory—before the first store (`str A`) does so. If a power outage occurs here, all volatile data—including `str A`—in the cache are lost, while only the data in the CMM-H are preserved as shown in Figure 2 (c). Once power is restored, the `next` pointer of the new node becomes dangling, as illustrated in Figure 2 (d), resulting in inconsistent program states.

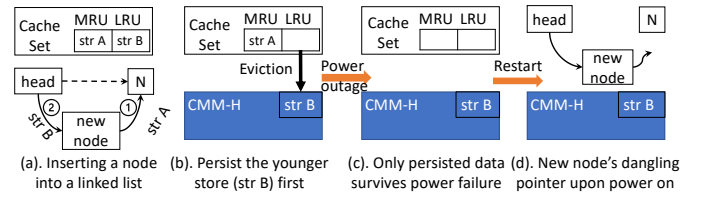


Fig. 2: Inconsistent program states for singly-linked list insertion across power failure; CMM-H device here functions as persistent memory

Figure 2 shows that the root cause of crash inconsistency is the loss of all volatile cache contents upon power failure. To address this, many techniques, e.g., extended asynchronous DRAM refresh (eADR) [62] and CXL Global Persistent Flush (GPF) [123], were proposed to include the entire cache hierarchy in persistent domain; assuming the main memory (i.e., CMM-H) is already in persistent domain. That way, a store becomes persisted as soon as its data is merged into the L1D cache. The beauty of this approach is that programmers can circumvent using expensive persist barriers—e.g., `clwb` and `sfence` in x86—which cause frequent pipeline stalls and result in significant performance loss.

Unfortunately, CXL GPF or eADR alone cannot guarantee crash consistency for user program. This is because volatile registers in the cores are still suffering from losing their data upon power outages, preventing applications from recovering. To address this issue, Zeng et al. [146] leverage compiler techniques to store (checkpoint) registers to persistent memory, which unifies register consistency with memory consistency. That way, each checkpoint location serves as a recovery point from which a power-interrupted program resumes its execution, forming a series of recoverable intervals and achieving interval-level crash consistency.

Nevertheless, checkpointing registers too often—i.e., short checkpointing intervals—incurs high performance overhead due to frequent write traffic towards memory; these checkpoints are essentially stores but exhibit poor locality, as the data is only accessed during recovery. On the other hand,

checkpointing registers too rarely—i.e., long checkpointing intervals—incur high recovery cost; once power is restored, the recovery runtime has to roll back the program execution to a distant previous checkpoint to recover the interrupted program, as all the register updates since the last checkpoint are lost. This renders the instruction execution since the last checkpoint wasted.

In addition, it is not always safe to re-execute program from the last checkpoint due to memory write-after-read (WAR) dependence—a.k.a antidependence [2]—which is prevalent in program code. That is, at recovery time, a checkpoint interval with memory WAR dependences may use updated memory data as input for its re-execution and thereby generates incorrect program output, resulting in failed program recovery. Prior approaches [132], [107], [73], [5], [70], [53], [68], [65] to this problem have to resort to logging techniques which amplify memory writes and rely on costly persist barriers. This is, it logs memory writes followed by persist barriers in case of power failure. For example, undo logging saves the old data of a store to a dedicated logging area in persistent memory before the store’s memory location is updated with the new data. When a power outage occurs, their recovery runtime reverts the memory update using the undo log, ensuring consistent memory states.

To address the above issue while maintaining a suitable interval length for low recovery overhead, Zeng et al. propose using an idempotent-processing-based compiler [88], [26], [28], [27], [75] to divide program into a series of idempotent regions (intervals)—which do not have memory WAR dependences. Because of this, these regions can be re-executed arbitrarily while generating the same output. Moreover, idempotent processing forms regions with moderate sizes, i.e., ≈ 40 instructions on average in idempotent regions [146], which enables a sweet spot between lower register checkpointing overhead and fast failure recovery. In particular, to further reduce checkpointing overhead, the compiler performs liveness analysis [2] to figure out each region’s live-out registers to be checkpointed. That way, upon power failure, an interrupted program can resume execution from the beginning of the power-interrupted region after reloading the region’s live-in registers from main memory. Consequently, CMM-H with idempotent processing together ensures crash consistency for user applications.

III. EVALUATION METHODOLOGY

A. System and Device Configurations

System Configurations: We conducted our experiments on an x86-64 dual-socket server (see Table I). Each socket has 48 AMD EPYC 9454 cores with hardware hyper-threading and frequency boost disabled. Each core is equipped with 32 kB L1I/L1D caches and a 1 MB L2 cache, and each CPU has a 256 MB L3 cache. The total DRAM main memory size is 512 GB with 256 GB per socket. We install Ubuntu 22.04.4 LTS with Linux kernel 6.8.0-49 on the server. All evaluated applications are compiled using the default GCC

11.4.0 compiler with default compilation flags unless noted otherwise.

Samsung CMM-H Configurations: As shown in Table II, we configure the 1 TB Samsung CMM-H as a CPU-less NUMA node so that it can be accessed by the cores without any changes to program source code. Within the CMM-H, the 1 TB NAND flash is connected to the DRAM cache through PCIe Gen4 x4. Here, the DRAM cache is 16 GB and is managed by an FPGA board working as a DRAM cache controller.

TABLE I: Host System Configurations

Component	Description
OS (Kernel)	Ubuntu 22.04 LTS (Linux kernel 6.8.0-49)
Compiler	GCC 11.4.0
CPU	2x AMD EPYC 9454 CPUs @2.75 GHz, 48 cores and 32 kB L1I/L1D caches, 1 MB L2 cache, and 256 MB LLC per CPU Hyper-Threading disabled
Memory	Socket 0: 8x DDR5-4800, 300 GB/s max. bandwidth Socket 1: 8x DDR5-4800, 300 GB/s max. bandwidth Socket 2: Samsung CMM-H
Disk	960 GB NVMe Samsung M.2 SSD
Host and Disk Connection	PCIe Gen4 x8

TABLE II: CMM-H Configurations

Component	Description
CXL	v1.1, CXL.io/CXL.mem (Type 3)
Device DRAM Cache	8-way, 4 KB cacheline, LRU replacement policy, MRU insertion policy, writeback, 16 GB DDR4-2666
NAND Flash	1 TB Samsung NAND SSD (TLC) [118]
Device Cache-NAND Flash Connection	PCIe Gen4 x4
Total Power	40 W, including FPGA-based controller, NAND flash, and DRAM Cache

B. Experimental Configurations

As depicted in Table I, Samsung’s CMM-H memory behaves like a CPU-less NUMA node and therefore can directly replace DRAM DIMMs as main memory without any software changes. In our study, we treat local DRAM memory (DDR5-L)—it is placed on the same socket as the core where the evaluated benchmarks run—as baseline and compare it with other configurations, e.g., remote DRAM memory (DDR5-R) and CMM-H. **Notably, we do not conduct experiments on Intel Optane memory as it is not supported on our AMD CPUs-based testbed.** To evaluate program performance on the servers equipped with multiple memory devices, we use a Linux command `numactl` to force page allocation accordingly and to bind user applications to a fixed CPU core.

C. Microbenchmarks

Thanks to the CXL-enabled byte addressability, the large-capacity CMM-H device now can be directly accessed with regular load/store instructions while alleviating any software changes. To demonstrate the impact of such a great feature on application performance, we conduct a thorough performance characterization of the CMM-H prototype. We employ two distinct microbenchmarks. The first is Intel Memory Latency Checker (MLC) v3.11b [24], which performs pointer-chasing

in a (1800 MB) memory region—it is larger than the LLC capacity—to measure memory latency. In addition, we follow prior approaches [126], [138] to characterize different memory devices—i.e., DDR5 and CMM-H—for four types of instructions: temporal load (`ld`), non-temporal load (`nt-ld`), temporal store (`st`), and non-temporal store (`nt-st`). This provides a comprehensive performance characterization of CMM-H, allowing for capturing key performance metrics that are critical for system designers and programmers.

D. Benchmarks

Volatile applications: First, we run SPEC CPU2017 [9], [87], [124], which is a classic performance evaluation tool for CPUs, memory systems, and compilers, to demonstrate how CMM-H affects program performance by replacing DRAM with CMM-H. To stress the memory system, we run the CPU2017 applications with reference data input and collect their execution time. Second, we execute LLaMA 3.c [29], a C version of popular large language models (LLMs), with varying thread count from 1 to 32 to showcase how it performs on CMM-H. Note that we feed the LLaMA 3 with llama3.2 1B model [97] as data input—whose memory footprint is 4740 MB—to isolate caching effect as much as possible and thus to stress the main memory. To mitigate the varying throughout of each run, we execute the LLaMA 3 program for each thread count 5 times and average their throughputs (tokens per second). Last, we run XSBench [129], a key computational kernel of the Monte Carlo neutron transport algorithm, to characterize the performance HPC program on the CMM-H. As XSBench provides a flexible way to adjust problem sizes and hence its memory footprint, we also use XSBench with varying problem sizes to characterize how the DRAM cache within the CMM-H prototype affects program performance; please see Section V-C for more details.

In-memory databases (persistent applications): As persistent memory, CMM-H obviates the need to periodically log program states to external slow storage devices. To demonstrate how such a feature boosts program performance, we select two typical in-memory databases, RocksDB 9.9.3 [98] and Redis 7.4.1 [116]. First, we run single-threaded `db_bench` on a specified memory device (e.g., DDR5-L) with varying operations (e.g., `fillseq` and `fillrandom`). For each run, we insert 1 million pair of key/values with their sizes set to 16 bytes and 100 bytes, respectively. We set block size and write buffer size to 4 kB and 64 MB by default, respectively. Likewise, we run Redis server on a specified memory device with a single thread and use `redis-benchmark` shipped with Redis as a client to benchmark the Redis server’s throughput (requests per second). To stress the memory, for each run, the `redis-benchmark`—running on the DDR5-L and local core—initiates 200000 requests with a key size of 10 kB and a random key length of 100000.

IV. BASIC LATENCY AND BANDWIDTH CHARACTERIZATION

In this section, we first characterize the load and store latencies of random accesses to the CMM-H device using the microbenchmarks described in Section III-C. We then evaluate CMM-H’s tail latency and bandwidth. With these experiments in mind, we draw key takeaways on programming for the CMM-H device.

A. Load and Store Latencies

Figure 3 reveals the normalized load and store latencies of remote DDR5 memory (DDR5-R) and CMM-H, relative to those of local DDR5 memory (DDR5-L). The first group of bars shows the latency measured using Intel MLC, which performs pointer-chasing operations in a memory region of 1800 MB; it is larger than the LLC size (i.e., 256MB per CPU). Intel MLC issues memory reads back-to-back, which essentially measures the latency of serialized memory reads.

The remaining four groups of Figure 3 show the latencies of four types of instructions: temporal load (`ld`), non-temporal load (`nt-ld`), temporal store (`st`), and non-temporal store (`nt-st`). Similar to prior approaches [138], [126], we measure the latency of each instruction type by issuing 16 64-byte memory accesses to the main memory. To avoid the impact of data locality as much as possible, each of these memory operations accesses a random cacheable location within the main memory. To ensure no interference with other instructions, we flush the entire core pipeline followed by a memory fence before issuing these memory instructions; they are also followed by a memory fence to ensure their completions. It is worth noting that these 16 memory accesses could be executed in parallel, therefore effectively measuring the latency of random parallel memory accesses for each instruction type on a given memory device. To accurately estimate the execution time of these memory operations, we use inline assembly code (i.e., `rdtsc` instruction in `x86_64`) to read the timestamp counter twice: once before issuing these memory operations and once after they complete. We then subtract the two readings to calculate the execution time of these 16 memory accesses. We repeat the procedure of pipeline flushing, executing 16 memory accesses, reading the timestamp counter 10000 times, and calculating the median number.

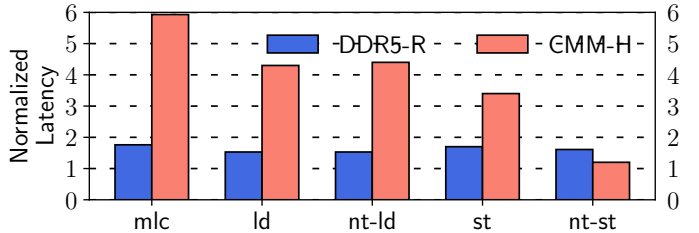


Fig. 3: Normalized random access latencies of DDR5-R and CMM-H to those of DDR5-L (local DRAM); lower is better

Figure 3 shows that CMM-H is slower than both DDR5-L and DDR5-R for MLC, `ld`, `nt-ld`, and `st`. This is

TABLE III: Median Latency (ns) of three Memory Devices

Memory Device	Intel MLC	ld	nt-ld	st	nt-st
DDR5-L	122.9	13.1	13.1	33.5	13.5
DDR5-R	216	20.0	20.0	56.7	21.8
CMM-H	728.9	56.7	57.5	114.9	16.0

expected because of the additional latency introduced by signal propagation over the PCIe link and CMM-H’s DRAM cache controller processing. Note that the latencies measured by Intel MLC are 9x-12x higher than those measured by ld for all three memory devices. As presented in Table III, for DDR5-L, Intel MLC reports a latency of 122.9 ns, while ld yields only 13.3 ns. This matches what prior work observed [126]: Intel MLC issues read operations back-to-back and hence cannot make use of the full-duplex PCIe link [122]. In contrast, ld does so by issuing 16 memory accesses in parallel, thereby overlapping their memory access latencies to some degree.

Key takeaways: Due to the FPGA-based DRAM cache controller and the unmodified NAND flash architecture designed for PCIe Gen4x4 SSDs, CMM-H incurs 1.2x to 5.9x higher latency compared to DDR5-L. This indicates that latency-sensitive workloads would suffer significant performance degradation if they rely on CMM-H as their sole main memory, as confirmed in Section V.

As the first two groups of bars contrast in Figure 3, CMM-H experiences a higher reduction in latency as the measurement switches from Intel MLC to ld; this is also observed in the first two columns of Table III. The reason, as discussed in prior work [126], is that the sequential memory accesses issued by Intel MLC result in a burst of cache-coherence related lookups in the remote CPU, which unfortunately introduces extra delays for DDR5-R accesses; each remote memory access needs to go through the remote CPU’s internal cache hierarchy to search for the corresponding cache block, and even worse the resulting latency goes up as the number of cores rises. On the contrary, accesses to CMM-H do not need to go through such time-consuming lookups due to the lack of inter-core connections and cache hierarchies within the CMM-H prototype.

The same explanation above is also applicable to the contrast between the ld bars and the st bars. As illustrated in the table, compared to DDR5-L, st causes a higher increase (i.e., 1.70x) in latency than ld (i.e., 1.53x) for DDR5-R. This contrasts with what is observed for CMM-H where st gives a 3.4x higher latency, whereas ld leads a 4.3x higher latency. This is because the execution of st instructions need to first implicitly perform memory read accesses (i.e., ld)—bring the corresponding cachelines from main memory to the L1D cache—for write-allocate writeback caches. Consequently, stores experience longer execution delays than loads on DDR5-R. On the other hand, the execution of st on CMM-H avoids the costly inter-socket cache-coherence lookups which are necessary for DDR5-R, and this latency saving outweighs the extra delay caused by the implicit memory read accesses.

Interestingly, as shown in the last two columns of Table III, nt-st is faster than st on all the three memory devices. This is because nt-st directly heads to main memory without going through multiple levels of cache hierarchy, whereas st implicitly requires a memory read access—doubling its execution latency of st—as discussed before. Moreover, nt-st performs even faster on CMM-H than on DDR5-R, due to absence of costly inter-socket cache-coherence lookups on CMM-H, which further lowers the execution latency of nt-st on CMM-H.

Key takeaways: nt-st performs significantly (i.e., 7x) better than st on CMM-H. This suggests that a potential way to boost the performance of applications with random (cache-unfriendly) writes is to replace temporal stores with non-temporal stores.

B. Tail Latency

In addition to basic load and store latencies, tail latency is also a critical factor that affects the worst-case performance of computing systems, as memory accesses may, in the worst case, be served from the slow backing NAND flash. For this reason, we follow the same methodology as prior work [138] to measure the 99.99th, 99.999th, and maximal latencies across varying memory region sizes. For each memory region size, a latency measurement program first flushes all the cachelines within the memory region and then clears the core pipeline by issuing a sufficient number of nop instructions. After that, the program generates 16 64-byte memory read accesses to random locations within the region. For each region size, we run the measurement program 20 million times.

Figure 4 and 5 show the tail latencies of DDR5-L and CMM-H, respectively, across varying memory region sizes—which the 16 memory reads access—from 1 MB to 32 GB. As depicted in Figure 4, the 99.99th and 99.999th latencies of DDR5-L are ≈ 300 ns and ≈ 750 ns, respectively, while the maximal latency of DDR5-L fluctuates between $300 \mu s$ and $400 \mu s$.

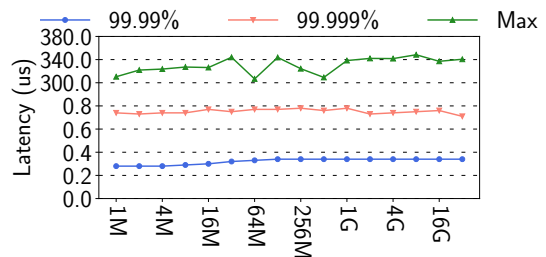


Fig. 4: Tail latency in microseconds of reads for DDR5-L across memory region sizes

Figure 5 shows that for CMM-H, the 99.99th, 99.999th, and maximal latencies are ≈ 450 ns, $\approx 1.8 \mu s$, and $\approx 400 \mu s$, respectively, which are higher than those of DDR5-L; its tail latency follows the same trend as Zhang *et al.* observed [148]. This is not surprising as CMM-H suffers from propagation delays over PCIe and processing overhead from the PoC’s FPGA-based DRAM cache controller. As expected,

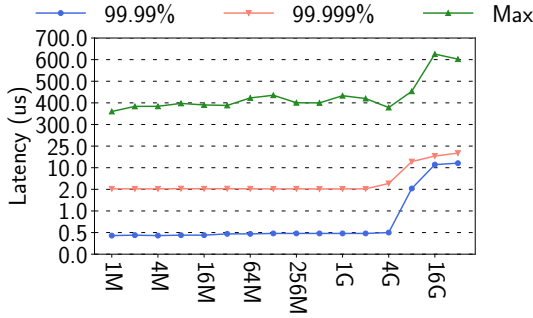


Fig. 5: Tail latency in microseconds of reads for CMM-H across memory region sizes

unlike DDR5-L, all three latencies of CMM-H rise quickly as the memory region size exceeds 4 GB. We suspect this is because the DRAM cache experiences significant conflict misses [54], exposing the long latency of the backend NAND flash to upper-level program due to the deficient DRAM cache associativity (i.e., 8). These latencies even reach $\approx 15 \mu s$, $\approx 20 \mu s$, and $\approx 600 \mu s$, respectively, when the region size rises up to 32 GB; please refer to Section V-C for detailed analysis.

Key takeaways: When a program’s memory footprint fits within CMM-H’s device DRAM cache, the 99.99th, 99.999th, and maximum latencies of CMM-H are comparable to those of DDR5-L. However, these latencies for CMM-H increase significantly once the memory footprint exceeds the device DRAM cache capacity.

C. Bandwidth

Memory bandwidth is another critical factor for performance; prior approaches [147], [66] have shown that higher memory bandwidth significantly improves the performance of bandwidth-sensitive program (e.g., HPC and ML workloads) since they typically run multiple threads on many cores to deliver high throughput. In this section, we measure the bandwidth of three instruction types (ld, st, and nt-st) following the methodology of prior studies [126], [138]. We exclude nt-ld from this experiment since its behavior is similar to that of ld. For sensitivity analysis, we vary the number of threads from 1 to 32. Specifically, we launch a given number of threads that execute one of the three instruction types to access 512 cachelines and sum the bandwidths across all threads. To maintain accuracy, we run the measurement program 10 times for each given thread count.

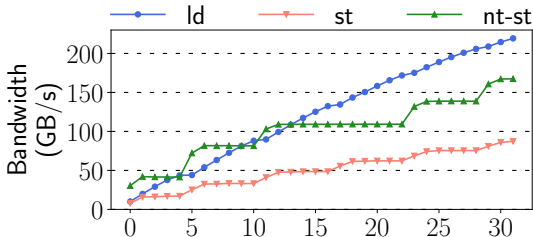


Fig. 6: Bandwidth of DDR5-L across 3 kinds of instructions with varying threads from 1 to 32; 64 bytes access size

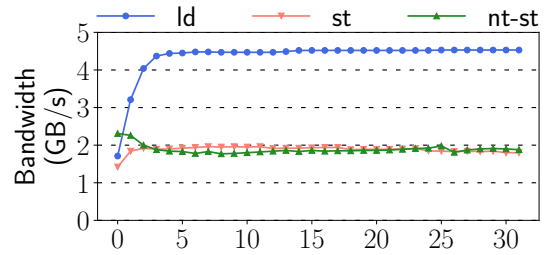


Fig. 7: Bandwidth of CMM-H across 3 kinds of instructions with varying threads from 1 to 32; 64 bytes access size

Figure 6 shows the bandwidth (in GB per second) of the three instruction types for DDR5-L. We conclude that (1) ld delivers higher bandwidth than the other two types of instructions, and (2) the bandwidths of these three instruction types scale well with increasing thread counts on DDR5.

Figure 7 shows the bandwidth of the three instruction types for CMM-H. The maximal bandwidths (i.e., 4.5GB/s) of all three instruction types running on CMM-H are significantly lower than those (i.e., 219GB/s) on DDR5-L. Moreover, the bandwidth of CMM-H for ld and st saturates at 4 and 2 threads, respectively. Even worse, the bandwidth of nt-st drops when the thread count exceeds four. These low bandwidth numbers suggest that the CMM-H’s internal DRAM cache controller and untailed NAND flash architecture significantly limits its performance.

Key takeaways: Compared to DDR5, the FPGA-based CMM-H has limited bandwidths, particularly for write operations. This limitation stems from the underlying unmodified NAND flash and could be overcome by employing a tailored NAND flash architecture that fully exploits available internal parallelism.

V. CHARACTERIZING CMM-H AS VOLATILE MEMORY

With the support for CXL-compliant interfaces, CMM-H can operate as a byte-addressable remote memory expansion. However, CMM-H with a hybrid design combining a DRAM cache and NAND flash cannot serve as the sole main memory for many applications. To understand whether a wide variety of applications can successfully run on CMM-H and whether doing so meets their economic needs, in this section, we evaluate several typical workloads, e.g., SPEC CPU2017 [9], LLaMA 3 [29], and XSBench [129], on CMM-H; For comparison, we also evaluate the workloads on DDR5-L and DDR5-R.

A. CPU2017

Figure 8 shows the normalized execution times of CPU2017 applications on DDR5-R and CMM-H, respectively, relative to those on DDR5-L; we evaluate all applications from CPU2017 except for wrf and cam4 due to compilation issues. As shown in the figure, CPU2017 gets slowed down by 12% and 70% on average when running on DDR5-R and CMM-H, respectively, compared to DDR5-L.

To better present the evaluation results, we organize the figure by categorizing the applications into three groups

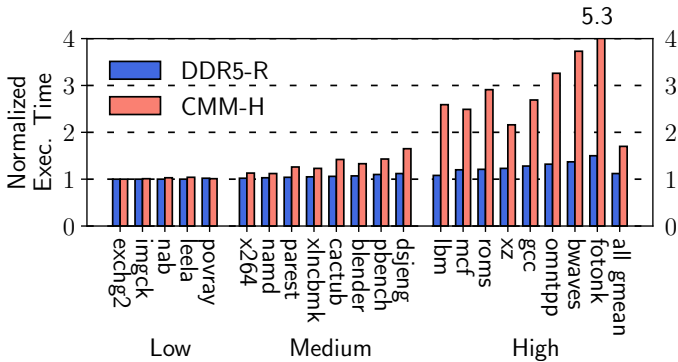


Fig. 8: Normalized execution times of CPU2017 applications on DDR5-R and CMM-H to those on DDR5-L (baseline); lower is better; the applications are grouped into three kinds according to their memory pressure

based on memory pressure: (1) low memory pressure, (2) medium memory pressure, and (3) high memory pressure, as shown in the figure. For applications—e.g., `exchange2` and `imagick`—with low memory pressure, whose working sets are small enough to fit in CPU’s private caches [124], both DDR5-R and CMM-H cause negligible performance loss, as their memory accesses hit the CPU caches most of time. On the other hand, applications like `parest` and `xalancbmk`, which have slightly larger working sets than the LLC size (256 MB), exhibit moderate memory pressure and hence run slightly ($\approx 5\%$) slower on DDR5-R. A similar trend is observed for CMM-H, although these applications experience greater slowdowns due to its higher latency than DDR5-R.

Nevertheless, as presented in the figure, applications like `mcf` and `bwaves` experience significant performance losses on both DDR5 and CMM-H. For example, `bwaves` suffers a 1.37x and 3.73x slowdown on DDR5-R and CMM-H, respectively. This is because these applications have large working sets, leading to high LLC misses, e.g., `bwaves` and `fotonick` suffer a 44% and 46% LLC miss rate on our test server, respectively, causing many of their memory accesses to be served by the slower CMM-H. Among these, `fotonick` gets degraded dramatically because of its irregular memory accesses, causing a 99.988% DRAM cache hit rate. Note that such a high DRAM cache hit rate still leads to a significant performance drop due to the wide speed gap between the DRAM cache and the backing NAND flash; see Section V-C for detailed analyses.

Key takeaways: Applications with smaller memory footprints can be fully supported on CMM-H alone, similar to DDR5-R, without any noticeable performance drops. However, other applications will require more intelligent solutions, such as OS/VMM enabled automatic memory tiering, to avoid noticeable losses.

B. LLaMA 3

LLaMA 3 [30], developed by Meta, marks a significant step forward in open-source large language model (LLM) technology. Building on the foundation established by LLaMA 2, this

version offers models with various numbers of parameters—e.g., 1 billion (1B), 8 billion (8B), and 70 billion (70B) parameters—available in both pre-trained and instruction-tuned configurations. To stress the memory system while keeping experiments manageable, we choose 1B model from LLaMA 3.2 [97] with a memory consumption of 4740 MB and an up to 97% LLC miss rate.

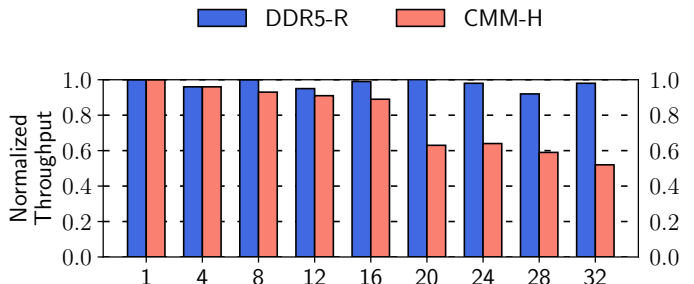


Fig. 9: Normalized throughput (tokens/second) of LLaMA 3 with varying threads from 1 to 32 on DDR5-R and CMM-H to that on DDR5-L; higher is better

From Figure 9, we can make two conclusions. First, memory latency has an insignificant impact on the throughput of LLaMA 3. This is because LLaMA 3’s throughput remains stable across thread counts on DDR5-R, although it is slower than DDR5-L by $\approx 50\%$ (see Figure 3 for details). Second, LLaMA 3’s throughput is highly affected by memory bandwidth. As shown in the figure, LLaMA 3’s performance loss gets larger as more threads run on CMM-H. For example, LLaMA 3 suffers a 4% and 48% slowdown in throughput with 4 and 32 threads, respectively. The reason is that CMM-H’s bandwidth saturates at four threads (see Figure 7) and more threads lead to higher bandwidth contention on the CMM-H prototype.

Key takeaways: Bandwidth-sensitive applications can benefit most from CMM-H memory expansion, if the applications are intelligent enough in consolidating duplicate requests and if the CMM-H architecture, including the backing NAND flash, is optimized for maximum bandwidth utilization.

C. XSBench

XSBench [129] is widely used in high-performance computing (HPC) research for performance evaluation and optimization of memory and compute-intensive tasks. XSBench mimics the irregular memory access patterns and computational intensity of full-scale Monte Carlo transport simulations, making it particularly valuable for studying the behavior of memory hierarchies and bandwidth under irregular access patterns.

In particular, XSBench offers users a way to configure problem sizes, such as the number of energy levels, isotopes, and lookups, therefore allowing users to adjust its memory footprint on demand; XSBench’s memory consumption is proportional to the problem size. By leveraging this flexible configuration, it becomes possible for us to analyze how the DRAM cache within CMM-H performs across varying

memory footprints. To achieve this, we select 10 different problem size configurations to stress CMM-H, especially for its internal DRAM cache. For example, as shown in Table IV, as the number of gridpoints per nuclide (specified by flag -g) increases from 160 to 81920, XSBench’s memory footprint starts from only 80 MB and increases up to 40 GB, which enables different levels of the memory hierarchy to be stressed. We run the single-threaded version of XSBench (specified by flag -t 1) to avoid bandwidth contention on the CMM-H.

Figure 10 shows XSBench’s normalized execution times on DDR5 and CMM-H, relative to those on DDR5-L, across the 10 configurations. As expected, the performance degradation of DDR5-R increases gradually with larger memory footprints. We attribute this stable performance degradation to the constant inter-socket latency which is paid to access DDR5-R.

TABLE IV: XSBench Configurations

Configuration	Data Input	Memory Footprint	DRAM Cache Hit Rate
A	-t 1 -g 160	80 MB	99.9679%
B	-t 1 -g 320	160 MB	99.965%
C	-t 1 -g 640	320 MB	99.9624%
D	-t 1 -g 1280	640 MB	99.9502%
E	-t 1 -g 2560	1279 MB	99.9229%
F	-t 1 -g 5120	2558 MB	99.8635%
G	-t 1 -g 10240	5117 MB	99.8055%
H	-t 1 -g 20480	10234 MB	99.7653%
I	-t 1 -g 40960	20468 MB	98.6661%
J	-t 1 -g 81920	40936 MB	97.6209%

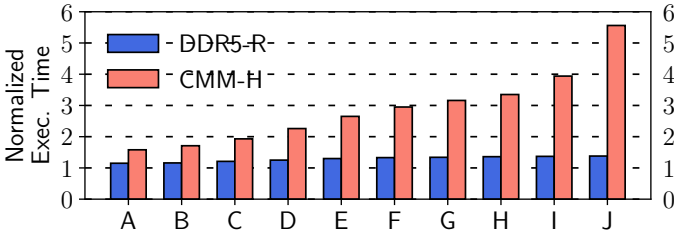


Fig. 10: Normalized execution times of XSBench on DDR5-R and CMM-H, relative to those on DDR5-L; lower is better; x-axis stands for differing problem sizes and hence varying memory footprints (see Table IV for details)

In contrast, the performance loss for CMM-H increases rapidly. For example, XSBench experiences a 1.58x performance loss when its memory footprint is only 80 MB (configuration A in Table IV). This performance loss goes up to 2.26x once the LLC cannot accommodate a memory footprint of 640 MB (configuration D in the table). As expected, performance loss remains the same level when the device DRAM cache can accommodate the memory footprint, e.g., under configurations F, G, and H, where the DRAM cache hit rate is consistently high as shown in the last column of Table IV. Once the memory footprint becomes larger than the device DRAM cache size (16 GB), the performance loss increases up to 3.94x and 5.56x for configurations I and J, respectively. This is due to extensive accesses to the significantly slow backing NAND flash. As shown in the last column of Table IV, the DRAM cache hit rate drops to only 97.6209% for

configuration J. Such a hit rate indicates that CMM-H’s latency is tens of times longer than that of the DRAM cache, given the significant ($\approx 500x$) speed gap between the backing NAND flash and the DRAM cache; a performance analysis report from Samsung[118] uncovers that the random read and write latencies of the backend NAND flash are on the order of tens of microseconds.

Key takeaways: Applications with irregular memory accesses and larger memory footprints than the DRAM cache capacity should expect to experience higher performance drops due to longer access latencies of the underlying NAND flash.

VI. CHARACTERIZING CMM-H AS MEMORY EXPANDER

Note that CMM-H is not intended as a replacement for DRAM technology, which would otherwise result in significant performance degradation due to its longer latency and lower bandwidth than DRAM. Instead, CMM-H is recommended to be used as a memory expansion solution to lower total cost of ownership (TCO). As shown in Table V, CMM-H achieves almost the same cost as conventional SSDs, making it 9.2x and 24x more cost-effective than DDR4 and DDR5, respectively.

TABLE V: Comparison of different memory devices

Memory Device	\$/GB	Persistence	Byte-Addressable
DDR4-2666	2.13	No	Yes
DDR5-4800	5.62	No	Yes
SSD	0.20	Yes	No
CMM-H	0.23	Yes	Yes

In addition, given that the performance of CMM-H is on par with DRAM, it is feasible to allocate part of program data to CMM-H without incurring significant performance degradation and at the same time enjoying lower TCO. To demonstrate this, we choose Redis with two typical operations, i.e., GET and SET, to test how their performance is affected by the amount of program data allocated to CMM-H. For this purpose, we switch Linux kernel to v6.12.12 such that we can use numactl with `-weighted-interleave` flag to specify the ratios of memory pages allocated to DDR5 and CMM-H. Table VI presents the normalized throughputs of Redis GET and SET operations under varying DDR5-to-CMM-H page allocation ratios compared to running the applications solely on DDR5-L. As shown in the table, CMM-H achieves 80% of DDR5-L’s performance when 50% of the pages are allocated to the DDR5-L.

TABLE VI: Normalized throughputs of Redis operations with part of program data allocated to CMM-H to those of running the operations only on DDR5-L

Redis Operation	75% DDR5-L: 25% CMM-H	67% DDR5-L: 33% CMM-H	50% DDR5-L: 50% CMM-H
GET	91%	88%	84%
SET	87%	82%	74%

As a result, using CMM-H as a memory expansion is expected to yield significant TCO savings, especially for

applications that do not always require large memory space for peak performance.

Key takeaways: CMM-H is ready to be used as a memory expander for those applications that do not always require large memory space for peak performance while incurring acceptable performance degradation and gaining significant TCO savings.

VII. CHARACTERIZING CMM-H AS PERSISTENT MEMORY

With CXL GPF [25], CMM-H works like persistent memory, i.e., it survives all volatile data in the DRAM cache from power failure. To show off how this feature enables higher performance for persistent program, in this section, we evaluate two popular in-memory databases, i.e., RocksDB [98] and Redis [116], which maintain key-value stores in memory for fast data operations.

As described in Section II-C, GPF alone cannot guarantee crash consistency. To address this issue, as with prior techniques [146], [88], [75], we use idempotent processing [26] to partition input program into a series of idempotent and thus recoverable regions; please refer to Section II-C for more details. Following a prior work [146], we implement idempotent processing on top of Clang/LLVM 13.0.1 [84] to build RocksDB 9.9.3 [98] and Redis 7.4.1 [116] from source code. To ensure recoverability for both workloads, we use the same compiler to build all the necessary runtime libraries, e.g., `glibc v2.27` [37], LLVM C++ library `libcxx` [40], LLVM `compiler-rt` [38], and LLVM stack unwinding library `libunwind` [39], and link the binaries of the RocksDB and Redis against those libraries.

It is worth noting that we pick idempotent processing among various crash consistency solutions due to its ability to transparently and automatically delineate recoverable regions. In contrast, other techniques, e.g., Intel PMDK [112], Atlas [15], and Clobber-NVM [137], require rewriting user source code with complex persistency models [110], [79] in mind, posing significant programming burden on users and potentially generating program bugs [90], [106], [89], [31].

A. RocksDB

RocksDB [98] is a high-performance key-value store developed by Facebook. Its core structure is an in-memory table called memtable which is technically a sorted data structure to accomplish efficient insertions and fast searches. When users issue a write request, the data being stored first goes into the memtable. To guarantee crash persistence in case of using DRAM as main memory, RocksDB also appends the data to a write-ahead log (WAL) file—residing in external storage—for failure recovery along with storing the data in the memtable, which however is considerably expensive.

To demonstrate how CMM-H benefits RocksDB by eliminating the expensive WAL, we run `db_bench` [13] for four configurations, DDR5-L, DDR5-R, CMM-H, and CMM-H (idem). We enable WAL for the original RocksDB running

on the former three memory devices, while disabling WAL for *idempotence-processed RocksDB* on the CMM-H. Figure 11 presents how RocksDB performs for these configurations. The x-axis indicates benchmarks from `db_bench`, while the y-axis stands for the normalized throughputs of these benchmarks to those on DDR5-L (baseline). *Note that CMM-H (idem) stands for the normalized throughputs of the benchmarks compiled by our idempotent compiler on the CMM-H; see Section II-C for the explanation of idempotent processing.*

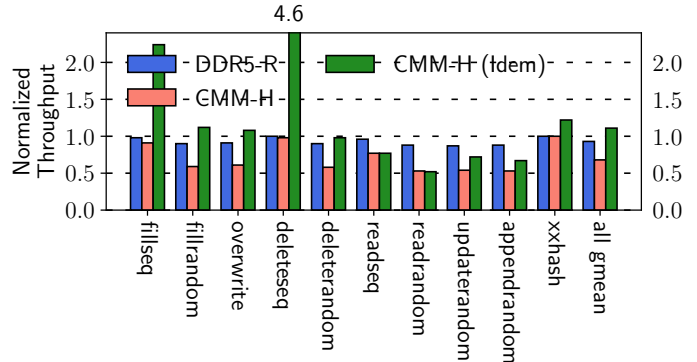


Fig. 11: Normalized throughputs of RocksDB on DDR5-R, CMM-H, and CMM-H (idem) to those on DDR5-L; higher is better; x-axis stands for RocksDB’s benchmarks

It is not surprising to see from the figure, that CMM-H leads to a higher performance slowdown than DDR5-L and DDR5-R. Due to longer latency and lower bandwidth, CMM-H (red bar in the figure) leads an average of 27% performance degradation, which is higher than only 7% of DDR5-R. In addition, we can see from the figure, CMM-H results in a significant performance loss (41%) for `fillrandom` which exhibits heavy random writes. This is because, due to randomness, `fillrandom` experiences high amount of misses in the DRAM cache. As such, a significant overhead is paid to access the backing NAND flash of the CMM-H prototype.

Nevertheless, DDR5-R and CMM-H lead to a marginal performance loss for benchmarks with heavy sequential writes. For example, there is no performance degradation observed for `fillseq` and `deleteseq` on DDR5-R as writes are usually not on the critical path. CMM-H results in an acceptable (i.e., 9%) slowdown for both benchmarks due to longer write latency (see Figure 7).

Key takeaways: Users should avoid performing random writes to CMM-H and instead employ intelligent software to coalesce them at page (4 kB) granularity. As such, the applications can benefit from page-level locality in the DRAM cache of the CMM-H prototype.

As reads are on the critical path of the core pipeline execution, a longer memory access latency could result in a severe performance loss. The figure shows that DDR5-R exhibits a 4% and 12% slowdown for sequential read (`readseq`) and random read (`readrandom`), respectively.

Of course, due to higher latency than DDR5, CMM-H leads to even higher performance degradations for those two operations; higher randomness results in poor data locality, which renders the DRAM cache ineffective. As such, the figure shows that `readseq` and `readrandom` observe a 23% and 47% performance loss, respectively.

Interestingly, despite being slower than DDR5-L and DDR5-R, CMM-H brings higher throughputs for write-intensive applications when it is enabled as persistent memory and the applications are idempotent. The figure shows that CMM-H boosts the throughputs of those evaluated programs by 11% on average; especially for `fillseq` and `deleteseq`, they witness a 2.2x and 4.59x speedup, respectively. The reason is twofold: (1) the slow CMM-H has marginal impact on those applications as they heavily use stores which are not on the critical path; (2) with idempotent processing and CXL GPF [42], those applications are crash-consistent, thereby obviating the need to use expensive write-ahead log (WAL).

Key takeaways: By obviating the need for expensive WAL, CMM-H with idempotent processing offers a chance to achieve significant performance gains for write-heavy applications, compared to the reliance on WAL to ensure crash consistency.

B. Redis

Redis [116] is another high-throughput in-memory key-value store commonly employed in website development as a caching layer and for message queuing applications. To ensure crash recovery, Redis logs all write operations to an append-only file (AOF), which is managed in DRAM main memory and periodically flushed to external storage devices based on a predefined flushing policy. Redis allows users to configure the frequency of AOF flushing to balance performance and consistency: higher flushing frequency improves recoverability but reduces performance due to increased interactions with external storage devices.

Specifically, Redis supports three AOF flushing modes: `always`, `everysec`, and `no`. In our experiments, we apply the default `always` flushing policy for DDR5-L, DDR5-R, and CMM-H (it is configured as volatile memory). This policy ensures that the AOF is flushed to external persistent devices after every log append, guaranteeing no data loss in the event of a crash. Conversely, for CMM-H (idem), we disable the logging and use the `no` flushing policy to eliminate the overhead of the logging. Instead, crash consistency is maintained through GPF [42] and idempotent processing, which work together to ensure data consistency without logging. By employing CMM-H (idem), we can estimate the potential performance gains that CMM-H can achieve for Redis.

Figure 12 shows the normalized throughputs of 12 applications for three memory configurations: DDR5-R, CMM-H, and CMM-H (idem). In the figure, the bars of DDR5-R and CMM-H represent the normalized throughputs of original Redis applications running on those two memory devices,

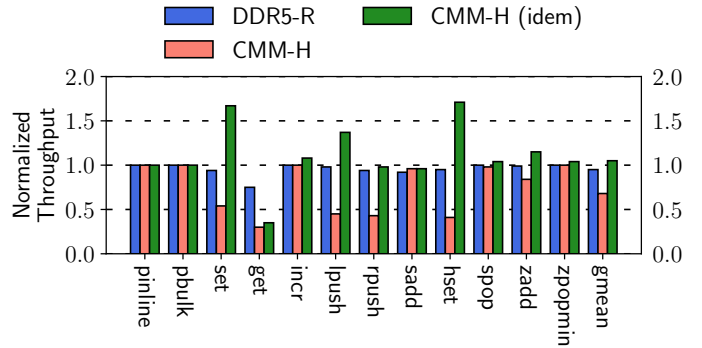


Fig. 12: Normalized throughputs of varying Redis applications on DDR5-R, CMM-H, and CMM-H (idem) to those on DDR5-L; higher is better; x-axis shows the applications from redis-benchmark

respectively, while CMM-H (idem) stands for the normalized throughputs of the *idempotent-processed* Redis applications with logging disabled on CMM-H.

As shown in the figure, CMM-H incurs a performance loss for memory-intensive applications, e.g., 46% for `set` and 70% for `get`. On the other hand, CMM-H leads to no observable negative performance impact on some applications, e.g., `pinline` (`ping_inline`), `pbulk` (`ping_bulk`), and `sadd`. We suspect this is because their memory accesses inherently hit in CPU caches, rendering those applications not sensitive to memory speed and bandwidth.

Key takeaways: Despite being slower than DRAM, CMM-H is a good fit for compute-intensive applications that exhibit high data locality and hence generate less frequent data accesses to main memory.

In particular, we can see from the figure, that with idempotent processing and GPF technique, CMM-H (idem) instead drastically improves the throughputs of some applications, such as 1.67x for `set`, 1.37x for `lpush`, and 1.71x for `hset`. This is because CMM-H (idem) could offset the lower performance of CMM-H by eliminating the expensive logging to external persistent devices. Even though CMM-H (idem) does not improve throughputs of other applications a lot, e.g., `rpush`, `spop`, and `zpopmin`, it offers these applications crash consistency and obviating the expensive logging, leading to shorter tail latency and ultimately improving user experience.

Key takeaways: As a replacement for the combination of DRAM and slower storage devices, CMM-H has the potential to be deployed in production environments for persistent applications to significantly boost their performance.

VIII. OTHER RELATED WORK

Compute Express Link (CXL) has emerged as a key enabling technology for memory expansion and pooling in modern datacenters. Extensive research has examined the po-

tential of CXL-based memory for disaggregated architectures [47], [67], [85], [48], [1], [133], [45]. Other research has investigated the role of CXL in tiered memory systems [96], [151], [154], [76], [120]. Notably, Meta has investigated using CXL for memory tiering [96], [135], while Microsoft has explored using CXL for memory disaggregation [6], [85] in production environments.

However, due to the limited availability of commercial CXL hardware, most studies rely on simulations and emulations for performance analysis [139], [134], [33], [42], [4]. While these studies provide valuable insights, they cannot fully capture the complexities of real-world deployments. To bridge this gap, several projects developed CXL hardware prototypes [48], [96], facilitating empirical evaluations and expanding our understanding of CXL’s potential in practical settings.

Nonvolatile memory (NVM) technologies, such as ReRAM [3], [16], PCM [77], [113], [119], [130], STT-MRAM [17], [57], [74], [80], 3D XPoint [52], Intel Optane memory (PMEM) [63], [121], [111], [64], [140], offer viable alternatives to DRAM. In this context, CXL has opened new opportunities to advance the performance of persistent memory and its adoption in modern computing systems [82], [42], [61]. TrainingCXL [82] is such an example that leverages CXL-enabled disaggregated memory to integrate persistent memory and GPUs within a cache-coherent domain. Additionally, Fridman et al. [42] explored the viability of CXL as a persistent memory solution for disaggregated high-performance computing, demonstrating its potential using an FPGA prototype with memory-backed DRAM. Samsung’s CMM-H prototype further exemplifies these advancements by combining a DRAM cache with NAND flash in a single device. Despite the innovations of CMM-H, the limited availability of publicly available performance characterizations has hindered its widespread adoption and the development of optimized programming practices. To address this gap, this paper presents the first comprehensive performance evaluation of the CMM-H prototype.

IX. CONCLUSION

This paper provides the first comprehensive performance evaluation of Samsung’s FPGA-based CMM-H prototype, which provides an economical way to significantly expand memory capacity while optionally offering persistence, compared to conventional memory technologies. To achieve high performance, CMM-H utilizes a DRAM cache to buffer hot data of its backend NAND flash. With extensive experiments and data analyses, this paper uncovers that CMM-H exhibits longer random memory access latency and limited bandwidth compared to both local DRAM and remote DRAM. Despite the longer random latency and lower bandwidth, CMM-H is able to deliver comparable performance for many popular applications. Nevertheless, applications with irregular memory access patterns and large memory footprints should account for the finite DRAM cache, as exceeding its capacity can lead to significant performance degradation.

It is worth noting that CMM-H’s advantages become prominent for persistent applications as it supports Global Persistent Flush (GPF) to flush the DRAM cache contents to the NAND flash upon power failure. For instance, CMM-H yields up to 4.6x and 1.7x throughput improvements for RocksDB and Redis, respectively. These performance gains primarily stem from the elimination of expensive logging to external storage devices by CMM-H and idempotent processing. Based on these experimental results, this paper offers key insights into how to best use the CMM-H device for both volatile and persistent applications.

REFERENCES

- [1] M. K. Aguilera, E. Amaro, N. Amit, E. Hunhoff, A. Yelam, and G. Zellweger, “Memory disaggregation: Why now and what are the challenges,” *ACM SIGOPS Operating Systems Review*, vol. 57, no. 1, pp. 38–46, 2023.
- [2] A. V. Aho, M. S. Lam, R. Sethi, and J. D. Ullman, *Compilers: principles, techniques, & tools*. Pearson Education India, 2007.
- [3] H. Akinaga and H. Shima, “Resistive random access memory (reram) based on metal oxides,” *Proceedings of the IEEE*, vol. 98, no. 12, pp. 2237–2251, 2010.
- [4] M. Arif, K. Assogba, M. M. Rafique, and S. Vazhkudai, “Exploiting cxl-based memory for distributed deep learning,” in *Proceedings of the 51st International Conference on Parallel Processing*, 2022, pp. 1–11.
- [5] J. Arulraj, M. Perron, and A. Pavlo, “Write-behind logging,” *Proceedings of the VLDB Endowment*, vol. 10, no. 4, pp. 337–348, 2016.
- [6] D. S. Berger, D. Ernst, H. Li, P. Zardoshti, M. Shah, S. Rajadnya, S. Lee, L. Hsu, I. Agarwal, M. D. Hill et al., “Design tradeoffs in cxl-based memory pools for public cloud platforms,” *IEEE Micro*, vol. 43, no. 2, pp. 30–38, 2023.
- [7] A. Bhattacharyya, A. Somashekhar, and J. S. Miguel, “Nvmr: non-volatile memory renaming for intermittent computing,” in *Proceedings of the 49th Annual International Symposium on Computer Architecture*, 2022, pp. 1–13.
- [8] B. Black, M. Annavaram, N. Brekelbaum, J. DeVale, L. Jiang, G. H. Loh, D. McCaule, P. Morrow, D. W. Nelson, D. Pantuso et al., “Die stacking (3d) microarchitecture,” in *2006 39th Annual IEEE/ACM International Symposium on Microarchitecture (MICRO’06)*. IEEE, 2006, pp. 469–479.
- [9] J. Bucek, K.-D. Lange, and J. v. Kistowski, “Spec cpu2017: Next-generation compute benchmark,” in *Companion of the 2018 ACM/SPEC International Conference on Performance Engineering*, 2018, pp. 41–42.
- [10] G. W. Burr and P. Franzon, “Storage class memory,” *Emerging Nano-electronic Devices*, pp. 498–510, 2014.
- [11] G. W. Burr, B. N. Kurdi, J. C. Scott, C. H. Lam, K. Gopalakrishnan, and R. S. Shenoy, “Overview of candidate device technologies for storage-class memory,” *IBM Journal of Research and Development*, vol. 52, no. 4.5, pp. 449–464, 2008.
- [12] Y. Cai, Y. Luo, E. F. Haratsch, K. Mai, and O. Mutlu, “Data retention in mlc nand flash memory: Characterization, optimization, and recovery,” in *2015 IEEE 21st International Symposium on High Performance Computer Architecture (HPCA)*. IEEE, 2015, pp. 551–563.
- [13] Z. Cao, S. Dong, S. Vemuri, and D. H. Du, “Characterizing, modeling, and benchmarking {RocksDB}{Key-Value} workloads at facebook,” in *18th USENIX Conference on File and Storage Technologies (FAST 20)*, 2020, pp. 209–223.
- [14] A. M. Caulfield, J. Coburn, T. Mollov, A. De, A. Akel, J. He, A. Jagatheesan, R. K. Gupta, A. Snaveley, and S. Swanson, “Understanding the impact of emerging non-volatile memories on high-performance, io-intensive computing,” in *SC’10: Proceedings of the 2010 ACM/IEEE International Conference for High Performance Computing, Networking, Storage and Analysis*. IEEE, 2010, pp. 1–11.
- [15] D. R. Chakrabarti, H.-J. Boehm, and K. Bhandari, “Atlas: Leveraging locks for non-volatile memory consistency,” *ACM SIGPLAN Notices*, vol. 49, no. 10, pp. 433–452, 2014.
- [16] Y. Chen, “Reram: History, status, and future,” *IEEE Transactions on Electron Devices*, vol. 67, no. 4, pp. 1420–1433, 2020.

- [17] P. Chi, S. Li, Y. Cheng, Y. Lu, S. H. Kang, and Y. Xie, "Architecture design with stt-ram: Opportunities and challenges," in *2016 21st Asia and South Pacific Design Automation Conference (ASP-DAC)*. IEEE, 2016, pp. 109–114.
- [18] A. Cho, A. Saxena, M. Qureshi, and A. Daglis, "Coaxial: A cxl-centric memory system for scalable servers," in *SC24: International Conference for High Performance Computing, Networking, Storage and Analysis*. IEEE, 2024, pp. 1–15.
- [19] J. Choi, L. Kittinger, Q. Liu, and C. Jung, "Compiler-directed high-performance intermittent computation with power failure immunity," in *2022 IEEE 28th Real-Time and Embedded Technology and Applications Symposium (RTAS)*. IEEE, 2022, pp. 40–54.
- [20] J. Choi, Q. Liu, and C. Jung, "Cospec: Compiler directed speculative intermittent computation," in *Proceedings of the 52nd Annual IEEE/ACM International Symposium on Microarchitecture*, 2019, pp. 399–412.
- [21] J. Choi, J. Zeng, D. Lee, C. Min, and C. Jung, "Write-light cache for energy harvesting systems," in *Proceedings of the 50th Annual International Symposium on Computer Architecture*, 2023, pp. 1–13.
- [22] J. Choi, J. Hong, Y. Kwon, and H. Han, "Libnvmio: Reconstructing software {IO} path with {Failure-Atomic}{Memory-Mapped} interface," in *2020 USENIX Annual Technical Conference (USENIX ATC 20)*, 2020, pp. 1–16.
- [23] C. M. Compagnoni, A. Goda, A. S. Spinelli, P. Feeley, A. L. Lacaita, and A. Visconti, "Reviewing the evolution of the nand flash technology," *Proceedings of the IEEE*, vol. 105, no. 9, pp. 1609–1633, 2017.
- [24] I. Corporation, "Intel memory latency checker v3.11b," <https://www.intel.com/content/www/us/en/developer/articles/tool/intelr-memory-latency-checker.html>, 2024.
- [25] D. Das Sharma, R. Blankenship, and D. Berger, "An introduction to the compute express link (cxl) interconnect," *ACM Computing Surveys*, vol. 56, no. 11, pp. 1–37, 2024.
- [26] M. De Kruijf and K. Sankaralingam, "Idempotent processor architecture," in *Proceedings of the 44th Annual IEEE/ACM International Symposium on Microarchitecture*, 2011, pp. 140–151.
- [27] —, "Idempotent code generation: Implementation, analysis, and evaluation," in *Proceedings of the 2013 IEEE/ACM International Symposium on Code Generation and Optimization (CGO)*. IEEE, 2013, pp. 1–12.
- [28] M. A. De Kruijf, K. Sankaralingam, and S. Jha, "Static analysis and compiler design for idempotent processing," in *Proceedings of the 33rd ACM SIGPLAN conference on Programming Language Design and Implementation*, 2012, pp. 475–486.
- [29] J. Delancey, "A c version of llama 3 llm architecture," <https://github.com/jameswdelancey/llama3.c>, 2024.
- [30] —, "Llama 3 in c language," <https://github.com/jameswdelancey/llama3.c>, 2024.
- [31] B. Di, J. Liu, H. Chen, and D. Li, "Fast, flexible, and comprehensive bug detection for persistent memory programs," in *Proceedings of the 26th ACM International Conference on Architectural Support for Programming Languages and Operating Systems*, 2021, pp. 503–516.
- [32] X. Dong, Y. Xie, N. Muralimanohar, and N. P. Jouppi, "Simple but effective heterogeneous main memory with on-chip memory controller support," in *SC'10: Proceedings of the 2010 ACM/IEEE International Conference for High Performance Computing, Networking, Storage and Analysis*. IEEE, 2010, pp. 1–11.
- [33] P. Esmaili-Dokht, F. Sgherzi, V. S. Girelli, I. Boixaderas, M. Carmin, A. Monemi, A. Armejach, E. Mercadal, G. Llort, P. Radojković *et al.*, "A mess of memory system benchmarking, simulation and application profiling," in *2024 57th IEEE/ACM International Symposium on Microarchitecture (MICRO)*. IEEE, 2024, pp. 136–152.
- [34] G. Fang, J. Choi, and C. Jung, "Hybrid power failure recovery for intermittent computing," in *ACM/IEEE International Conference on Computer-Aided Design (ICCAD)*, 2024.
- [35] G. Fang and C. Jung, "Rethinking dead block prediction for intermittent computing," in *2025 31st IEEE International Symposium on High-Performance Computer Architecture (HPCA)*. IEEE, 2025.
- [36] G. Fang, J. Zeng, A. Gupta, and C. Jung, "Rethinking prefetching for intermittent computing," in *2025 52th International ACM/IEEE Symposium on Computer Architecture (ISCA)*. ACM, 2025.
- [37] F. S. Foundation, "Gnu c standard library," <https://www.gnu.org/software/libc>, 2024.
- [38] L. Foundation, "compiler-rt runtime libraries," <https://compiler-rt.llvm.org>, 2024.
- [39] —, "A llvm-compatible unwinder," <https://bcain-llvm.readthedocs.io/projects/libunwind/en/latest>, 2024.
- [40] —, "A new c++ standard library for llvm," <https://libcxx.llvm.org>, 2024.
- [41] G. R. Fox, R. Bailey, W. B. Kraus, F. Chu, S. Sun, and T. Davenport, "The current status of feram," in *Ferroelectric Random Access Memories: Fundamentals and Applications*. Springer, 2004, pp. 139–148.
- [42] Y. Fridman, S. Mutalik Desai, N. Singh, T. Willhalm, and G. Oren, "Cxl memory as persistent memory for disaggregated hpc: A practical approach," in *Proceedings of the SC'23 Workshops of The International Conference on High Performance Computing, Network, Storage, and Analysis*, 2023, pp. 983–994.
- [43] A. Gholami, Z. Yao, S. Kim, C. Hooper, M. W. Mahoney, and K. Keutzer, "Ai and memory wall," *IEEE Micro*, 2024.
- [44] S. Ghose, A. G. Yaglikçi, R. Gupta, D. Lee, K. Kudrolli, W. X. Liu, H. Hassan, K. K. Chang, N. Chatterjee, A. Agrawal *et al.*, "What your dram power models are not telling you: Lessons from a detailed experimental study," *Proceedings of the ACM on Measurement and Analysis of Computing Systems*, vol. 2, no. 3, pp. 1–41, 2018.
- [45] C. Giannoula, K. Huang, J. Tang, N. Koziris, G. Goumas, Z. Chishti, and N. Vijaykumar, "Daemon: Architectural support for efficient data movement in fully disaggregated systems," *Proceedings of the ACM on Measurement and Analysis of Computing Systems*, vol. 7, no. 1, pp. 1–36, 2023.
- [46] A. Goda, "Recent progress on 3d nand flash technologies," *Electronics*, vol. 10, no. 24, p. 3156, 2021.
- [47] D. Gouk, M. Kwon, H. Bae, S. Lee, and M. Jung, "Memory pooling with cxl," *IEEE Micro*, vol. 43, no. 2, pp. 48–57, 2023.
- [48] D. Gouk, S. Lee, M. Kwon, and M. Jung, "Direct access, {High-Performance} memory disaggregation with {DirectCXL}," in *2022 USENIX Annual Technical Conference (USENIX ATC 22)*, 2022, pp. 287–294.
- [49] L. M. Grupp, J. D. Davis, and S. Swanson, "The bleak future of nand flash memory," in *FAST*, vol. 7, no. 3.2, 2012, pp. 10–2.
- [50] D. Habicht, Y. Khalil, L. Werling, T. Gröninger, and F. Bellosa, "Fundamental os design considerations for cxl-based hybrid ssds," in *Proceedings of the 2nd Workshop on Disruptive Memory Systems*, 2024, pp. 51–59.
- [51] R. Hadidi, B. Asgari, B. A. Mudassar, S. Mukhopadhyay, S. Yalamanchili, and H. Kim, "Demystifying the characteristics of 3d-stacked memories: A case study for hybrid memory cube," in *2017 IEEE international symposium on Workload characterization (IISWC)*. IEEE, 2017, pp. 66–75.
- [52] F. T. Hady, A. Foong, B. Veal, and D. Williams, "Platform storage performance with 3d xpoint technology," *Proceedings of the IEEE*, vol. 105, no. 9, pp. 1822–1833, 2017.
- [53] M. Haubenschild, C. Sauer, T. Neumann, and V. Leis, "Rethinking logging, checkpoints, and recovery for high-performance storage engines," in *Proceedings of the 2020 ACM SIGMOD International Conference on Management of Data*, 2020, pp. 877–892.
- [54] M. D. Hill and A. J. Smith, "Evaluating associativity in cpu caches," *IEEE Transactions on Computers*, vol. 38, no. 12, pp. 1612–1630, 1989.
- [55] J. Hong, S. Cho, G. Park, W. Yang, Y.-H. Gong, and G. Kim, "Bandwidth-effective dram cache for gpu s with storage-class memory," in *2024 IEEE International Symposium on High-Performance Computer Architecture (HPCA)*. IEEE, 2024, pp. 139–155.
- [56] W. W. Hsu and A. J. Smith, "The performance impact of i/o optimizations and disk improvements," *IBM Journal of Research and Development*, vol. 48, no. 2, pp. 255–289, 2004.
- [57] Y. Huai *et al.*, "Spin-transfer torque mram (stt-mram): Challenges and prospects," *AAPPS bulletin*, vol. 18, no. 6, pp. 33–40, 2008.
- [58] C.-C. Huang and V. Nagarajan, "Atcache: Reducing dram cache latency via a small sram tag cache," in *Proceedings of the 23rd international conference on Parallel architectures and compilation*, 2014, pp. 51–60.
- [59] S.-Y. Huang, J. Zeng, X. Deng, S. Wang, A. Sifat, B. Bharmal, J.-B. Huang, R. Williams, H. Zeng, and C. Jung, "Rtailor: Parameterizing soft error resilience for mixed-criticality real-time systems," in *2023 IEEE Real-Time Systems Symposium (RTSS)*. IEEE, 2023, pp. 344–357.
- [60] X. Huang, C. Liu, Y.-G. Jiang, and P. Zhou, "In-memory computing to break the memory wall," *Chinese Physics B*, vol. 29, no. 7, p. 078504, 2020.

- [61] S. S. Inc., “Industry’s 1st cxl-based storage optimized for ai/ml,” <https://semiconductor.samsung.com/us/about-us/us-office/us-r-and-d-labs/memory-labs/cxl-memory-module-hybrid/>, 2024.
- [62] I. Incorporation, “eadr: New opportunities for persistent memory applications,” <https://www.intel.com/content/www/us/en/developer/articles/technical/eadr-new-opportunities-for-persistent-memory-applications.html>, 2021.
- [63] Intel, “Intel optane persistent memory,” <https://www.intel.com/content/www/us/en/products/docs/memory-storage/optane-persistent-memory/overview.html>, 2019.
- [64] —, “Why Is the Intel Optane Persistent Memory in Memory Mode Not Persistent?” <https://www.intel.com/content/www/us/en/support/articles/000055895/memory-and-storage/intel-optane-persistent-memory.html>, 2019.
- [65] J. Izraelevitz, T. Kelly, and A. Kolli, “Failure-atomic persistent memory updates via justdo logging,” *ACM SIGARCH Computer Architecture News*, vol. 44, no. 2, pp. 427–442, 2016.
- [66] M. Jalili, I. Manousakis, I. Goiri, P. A. Misra, A. Raniwala, H. Alissa, B. Ramakrishnan, P. Tuma, C. Belady, M. Fontoura, and R. Bianchini, “Cost-efficient overclocking in immersion-cooled datacenters,” in *2021 ACM/IEEE 48th Annual International Symposium on Computer Architecture (ISCA)*, 2021, pp. 623–636.
- [67] J. Jang, H. Choi, H. Bae, S. Lee, M. Kwon, and M. Jung, “{CXL-ANNS}: {Software-Hardware} collaborative memory disaggregation and computation for {Billion-Scale} approximate nearest neighbor search,” in *2023 USENIX Annual Technical Conference (USENIX ATC 23)*, 2023, pp. 585–600.
- [68] J. Jeong, J. Hong, S. Maeng, C. Jung, and Y. Kwon, “Unbounded hardware transactional memory for a hybrid dram/nvm memory system,” in *2020 53rd Annual IEEE/ACM International Symposium on Microarchitecture (MICRO)*. IEEE, 2020, pp. 525–538.
- [69] J. Jeong and C. Jung, “Pmem-spec: persistent memory speculation (strict persistency can trump relaxed persistency),” in *Proceedings of the 26th ACM International Conference on Architectural Support for Programming Languages and Operating Systems*, 2021, pp. 517–529.
- [70] J. Jeong, C. H. Park, J. Huh, and S. Maeng, “Efficient hardware-assisted logging with asynchronous and direct-update for persistent memory,” in *2018 51st Annual IEEE/ACM International Symposium on Microarchitecture (MICRO)*. IEEE, 2018, pp. 520–532.
- [71] J. Jeong, J. Zeng, and C. Jung, “Capri: Compiler and architecture support for whole-system persistence,” in *Proceedings of the 31st International Symposium on High-Performance Parallel and Distributed Computing*, 2022, pp. 71–83.
- [72] M. I. Jordan and T. M. Mitchell, “Machine learning: Trends, perspectives, and prospects,” *Science*, vol. 349, no. 6245, pp. 255–260, 2015.
- [73] A. Joshi, V. Nagarajan, S. Viglas, and M. Cintra, “Atom: Atomic durability in non-volatile memory through hardware logging,” in *2017 IEEE International Symposium on High Performance Computer Architecture (HPCA)*. IEEE, 2017, pp. 361–372.
- [74] A. Khvalkovskiy, D. Apalkov, S. Watts, R. Chepulskii, R. Beach, A. Ong, X. Tang, A. Driskill-Smith, W. Butler, P. Visscher *et al.*, “Basic principles of st-mram cell operation in memory arrays,” *Journal of Physics D: Applied Physics*, vol. 46, no. 7, p. 074001, 2013.
- [75] H. Kim, J. Zeng, Q. Liu, M. Abdel-Majeed, J. Lee, and C. Jung, “Compiler-directed soft error resilience for lightweight gpu register file protection,” in *Proceedings of the 41st ACM SIGPLAN Conference on Programming Language Design and Implementation*, 2020, pp. 989–1004.
- [76] K. Kim, H. Kim, J. So, W. Lee, J. Im, S. Park, J. Cho, and H. Song, “Smt: Software-defined memory tiering for heterogeneous computing systems with cxl memory expander,” *IEEE Micro*, vol. 43, no. 2, pp. 20–29, 2023.
- [77] N. S. Kim, C. Song, W. Y. Cho, J. Huang, and M. Jung, “LI-pcm: Low-latency phase change memory architecture,” in *Proceedings of the 56th Annual Design Automation Conference 2019*, 2019, pp. 1–6.
- [78] S. K. Kim, G.-J. Choi, S. Y. Lee, M. Seo, S. W. Lee, J. H. Han, H.-S. Ahn, S. Han, and C. S. Hwang, “Al-doped tio2 films with ultralow leakage currents for next generation dram capacitors,” *Advanced Materials*, vol. 20, no. 8, pp. 1429–1435, 2008.
- [79] A. Kolli, V. Gogte, A. Saidi, S. Diestelhorst, P. M. Chen, S. Narayanasamy, and T. F. Wenisch, “Language-level persistency,” in *Proceedings of the 44th Annual International Symposium on Computer Architecture*, 2017, pp. 481–493.
- [80] K. Korgaonkar, I. Bhati, H. Liu, J. Gaur, S. Manipatruni, S. Subramoney, T. Karnik, S. Swanson, I. Young, and H. Wang, “Density tradeoffs of non-volatile memory as a replacement for sram based last level cache,” in *2018 ACM/IEEE 45th Annual International Symposium on Computer Architecture (ISCA)*. IEEE, 2018, pp. 315–327.
- [81] E. Kültürsay, M. Kandemir, A. Sivasubramaniam, and O. Mutlu, “Evaluating stt-ram as an energy-efficient main memory alternative,” in *2013 IEEE International Symposium on Performance Analysis of Systems and Software (ISPASS)*. IEEE, 2013, pp. 256–267.
- [82] M. Kwon, J. Jang, H. Choi, S. Lee, and M. Jung, “Failure tolerant training with persistent memory disaggregation over cxl,” *IEEE Micro*, vol. 43, no. 2, pp. 66–75, 2023.
- [83] Y. Kwon and M. Rhu, “Beyond the memory wall: A case for memory-centric hpc system for deep learning,” in *2018 51st Annual IEEE/ACM International Symposium on Microarchitecture (MICRO)*. IEEE, 2018, pp. 148–161.
- [84] C. Latner and V. Adve, “Llvm: A compilation framework for lifelong program analysis & transformation,” in *International symposium on code generation and optimization, 2004. CGO 2004*. IEEE, 2004, pp. 75–86.
- [85] H. Li, D. S. Berger, L. Hsu, D. Ernst, P. Zardoshti, S. Novakovic, M. Shah, S. Rajadnya, S. Lee, I. Agarwal *et al.*, “Pond: Cxl-based memory pooling systems for cloud platforms,” in *Proceedings of the 28th ACM International Conference on Architectural Support for Programming Languages and Operating Systems, Volume 2*, 2023, pp. 574–587.
- [86] S. Liang, Z. Qiao, S. Tang, J. Hochstetler, S. Fu, W. Shi, and H.-B. Chen, “An empirical study of quad-level cell (qlc) nand flash ssds for big data applications,” in *2019 IEEE International Conference on Big Data (Big Data)*. IEEE, 2019, pp. 3676–3685.
- [87] A. Limaye and T. Adegbiya, “A workload characterization of the spec cpu2017 benchmark suite,” in *2018 IEEE International Symposium on Performance Analysis of Systems and Software (ISPASS)*. IEEE, 2018, pp. 149–158.
- [88] Q. Liu, J. Izraelevitz, S. K. Lee, M. L. Scott, S. H. Noh, and C. Jung, “ido: Compiler-directed failure atomicity for nonvolatile memory,” in *2018 51st Annual IEEE/ACM International Symposium on Microarchitecture (MICRO)*. IEEE, 2018, pp. 258–270.
- [89] S. Liu, K. Seemakhupt, Y. Wei, T. Wenisch, A. Kolli, and S. Khan, “Cross-failure bug detection in persistent memory programs,” in *Proceedings of the Twenty-Fifth International Conference on Architectural Support for Programming Languages and Operating Systems*, 2020, pp. 1187–1202.
- [90] S. Liu, Y. Wei, J. Zhao, A. Kolli, and S. Khan, “Pmtest: A fast and flexible testing framework for persistent memory programs,” in *Proceedings of the Twenty-Fourth International Conference on Architectural Support for Programming Languages and Operating Systems*, 2019, pp. 411–425.
- [91] X. Liu, M. Zhou, R. Ausavarungnirun, S. Eilert, A. Akel, T. Rosing, V. Narayanan, and J. Zhao, “Fpra: A fine-grained parallel t1ram architecture,” in *2021 IEEE/ACM International Symposium on Low Power Electronics and Design (ISLPED)*. IEEE, 2021, pp. 1–6.
- [92] X. Liu, M. Zhou, T. S. Rosing, and J. Zhao, “Hr 3 am: A heat resilient design for rram-based neuromorphic computing,” in *2019 IEEE/ACM International Symposium on Low Power Electronics and Design (ISLPED)*. IEEE, 2019, pp. 1–6.
- [93] G. H. Loh and M. D. Hill, “Efficiently enabling conventional block sizes for very large die-stacked dram caches,” in *Proceedings of the 44th Annual IEEE/ACM International Symposium on Microarchitecture*, 2011, pp. 454–464.
- [94] G. H. Loh, Y. Xie, and B. Black, “Processor design in 3d die-stacking technologies,” *Ieee Micro*, vol. 27, no. 3, pp. 31–48, 2007.
- [95] J. A. Mandelman, R. H. Dennard, G. B. Bronner, J. K. DeBrosse, R. Divakaruni, Y. Li, and C. J. Radens, “Challenges and future directions for the scaling of dynamic random-access memory (dram),” *IBM Journal of Research and Development*, vol. 46, no. 2.3, pp. 187–212, 2002.
- [96] H. A. Maruf, H. Wang, A. Dhanotia, J. Weiner, N. Agarwal, P. Bhat-tacharya, C. Petersen, M. Chowdhury, S. Kanaujia, and P. Chauhan, “Tpp: Transparent page placement for cxl-enabled tiered-memory,” in *Proceedings of the 28th ACM International Conference on Architectural Support for Programming Languages and Operating Systems, Volume 3*, 2023, pp. 742–755.
- [97] I. Meta Platforms, “A 1 billion parameters model for llama 3,” <https://huggingface.co/meta-llama/Llama-3.2-1B>, 2024.

- [98] —, “A library that provides an embeddable, persistent key-value store for fast storage,” <https://rocksdb.org/>, 2024.
- [99] R. Micheloni, L. Crippa, and A. Marelli, *Inside NAND flash memories*. Springer Science & Business Media, 2010.
- [100] N. R. Mielke, R. E. Frickey, I. Kalastirsky, M. Quan, D. Ustinov, and V. J. Vasudevan, “Reliability of solid-state drives based on nand flash memory,” *Proceedings of the IEEE*, vol. 105, no. 9, pp. 1725–1750, 2017.
- [101] T. Mikolajick, C. Dehm, W. Hartner, I. Kasko, M. J. Kastner, N. Nagel, M. Moert, and C. Mazure, “Ferromagnetic technology for high density applications,” *Microelectronics Reliability*, vol. 41, no. 7, pp. 947–950, 2001.
- [102] Z. Milosevic, W. Chen, A. Berry, F. A. Rabhi, R. Buyya, R. Calheiros, and A. Dastjerdi, “Real-time analytics,” *Big Data: Principles and Paradigms*, vol. 2016, pp. 39–61, 2016.
- [103] K. Mizoguchi, T. Takahashi, S. Aritome, and K. Takeuchi, “Data-retention characteristics comparison of 2d and 3d tlc nand flash memories,” in *2017 IEEE International Memory Workshop (IMW)*. IEEE, 2017, pp. 1–4.
- [104] O. Mutlu, “Memory scaling: A systems architecture perspective,” in *2013 5th IEEE International Memory Workshop*. IEEE, 2013, pp. 21–25.
- [105] N. Nagel, T. Mikolajick, I. Kasko, W. Hartner, M. Moert, C.-U. Pinnow, C. Dehm, and C. Mazure, “An overview of ferromagnetic technology for high density applications,” *MRS Online Proceedings Library (OPL)*, vol. 655, pp. CC1–1, 2000.
- [106] I. Neal, A. Quinn, and B. Kasikci, “Hippocrates: Healing persistent memory bugs without doing any harm,” in *Proceedings of the 26th ACM International Conference on Architectural Support for Programming Languages and Operating Systems*, 2021, pp. 401–414.
- [107] M. A. Ogleari, E. L. Miller, and J. Zhao, “Steal but no force: Efficient hardware undo+ redo logging for persistent memory systems,” in *2018 IEEE International Symposium on High Performance Computer Architecture (HPCA)*. IEEE, 2018, pp. 336–349.
- [108] B. Oh, N. Abeyratne, N. S. Kim, J. Ahn, R. G. Dreslinski, and T. Mudge, “Rethinking dram’s page mode with stt-mram,” *IEEE Transactions on Computers*, 2022.
- [109] A. Papagiannis, G. Xanthakis, G. Saloustros, M. Marazakis, and A. Bilas, “Optimizing memory-mapped {I/O} for fast storage devices,” in *2020 USENIX Annual Technical Conference (USENIX ATC 20)*, 2020, pp. 813–827.
- [110] S. Pelley, P. M. Chen, and T. F. Wenisch, “Memory persistency,” *ACM SIGARCH Computer Architecture News*, vol. 42, no. 3, pp. 265–276, 2014.
- [111] I. B. Peng, M. B. Gokhale, and E. W. Green, “System evaluation of the intel optane byte-addressable nvm,” in *Proceedings of the International Symposium on Memory Systems*, 2019, pp. 304–315.
- [112] pmem.io, “Persistent Memory Development Kit,” <http://pmem.io/pmdk/>, 2017.
- [113] M. K. Qureshi, J. Karidis, M. Franceschini, V. Srinivasan, L. Lastras, and B. Abali, “Enhancing lifetime and security of pcm-based main memory with start-gap wear leveling,” in *2009 42nd Annual IEEE/ACM international symposium on microarchitecture (MICRO)*. IEEE, 2009, pp. 14–23.
- [114] M. K. Qureshi and G. H. Loh, “Fundamental latency trade-off in architecting dram caches: Outperforming impractical sram-tags with a simple and practical design,” in *2012 45th Annual IEEE/ACM International Symposium on Microarchitecture*. IEEE, 2012, pp. 235–246.
- [115] Z. Qureshi, V. S. Malthody, S. W. Min, I. Chung, J. Xiong, W.-m. Hwu *et al.*, “Tearing down the memory wall,” *arXiv preprint arXiv:2008.10169*, 2020.
- [116] redis.io, “An in-memory database that persists on disk,” <https://redis.io/>, 2024.
- [117] J. Ren, J. Zhao, S. Khan, J. Choi, Y. Wu, and O. Mutlu, “Thynvm: Enabling software-transparent crash consistency in persistent memory systems,” in *Proceedings of the 48th International Symposium on Microarchitecture*, 2015, pp. 672–685.
- [118] S. Semiconductor, “Samsung ssd pm9a3 specification,” https://www.ssd.group/wp-content/uploads/2022/07/PM9A3-NVMe-U-2-Datasheet_for-07_v1.4.pdf, 2021.
- [119] D. Sengupta, Q. Wang, H. Volos, L. Cherkasova, J. Li, G. Magalhaes, and K. Schwan, “A framework for emulating non-volatile memory systems with different performance characteristics,” in *Proceedings of the 6th ACM/SPEC International Conference on Performance Engineering*, 2015, pp. 317–320.
- [120] S. Sha, C. Li, Y. Luo, X. Wang, and Z. Wang, “vtmm: Tiered memory management for virtual machines,” in *Proceedings of the Eighteenth European Conference on Computer Systems*, 2023, pp. 283–297.
- [121] A. Shanbhag, N. Tatbul, D. Cohen, and S. Madden, “Large-scale in-memory analytics on intel® optane™ dc persistent memory,” in *Proceedings of the 16th International Workshop on Data Management on New Hardware*, 2020, pp. 1–8.
- [122] D. D. Sharma, “Compute express link (cxl): Enabling heterogeneous data-centric computing with heterogeneous memory hierarchy,” *IEEE Micro*, vol. 43, no. 2, pp. 99–109, 2022.
- [123] D. D. Sharma, R. Blankenship, and D. S. Berger, “An introduction to the compute express link (cxl) interconnect,” *arXiv preprint arXiv:2306.11227*, 2023.
- [124] S. Singh and M. Awasthi, “Memory centric characterization and analysis of spec cpu2017 suite,” in *Proceedings of the 2019 ACM/SPEC International Conference on Performance Engineering*, 2019, pp. 285–292.
- [125] N. Y. Song, Y. Son, H. Han, and H. Y. Yeom, “Efficient memory-mapped i/o on fast storage device,” *ACM Transactions on Storage (TOS)*, vol. 12, no. 4, pp. 1–27, 2016.
- [126] Y. Sun, Y. Yuan, Z. Yu, R. Kuper, C. Song, J. Huang, H. Ji, S. Agarwal, J. Lou, I. Jeong *et al.*, “Demystifying cxl memory with genuine cxl-ready systems and devices,” in *Proceedings of the 56th Annual IEEE/ACM International Symposium on Microarchitecture*, 2023, pp. 105–121.
- [127] D. Takashima, “Overview of ferams: Trends and perspectives,” in *2011 11th Annual Non-Volatile Memory Technology Symposium Proceeding*. IEEE, 2011, pp. 1–6.
- [128] M. Technology, “Micron NVDIMMs: Persistent Memory Performance,” <https://www.micron.com/content/dam/micron/global/public/products/product-flyer/nvdimm-flyer.pdf>, 2024.
- [129] J. R. Tramm, A. R. Siegel, T. Islam, and M. Schulz, “Xsbench—the development and verification of a performance abstraction for monte carlo reactor analysis,” *The Role of Reactor Physics toward a Sustainable Future (PHYSOR)*, 2014.
- [130] V. V. Tyagi and D. Buddhi, “Pcm thermal storage in buildings: A state of art,” *Renewable and sustainable energy reviews*, vol. 11, no. 6, pp. 1146–1166, 2007.
- [131] J. S. Vetter and S. Mittal, “Opportunities for nonvolatile memory systems in extreme-scale high-performance computing,” *Computing in Science & Engineering*, vol. 17, no. 2, pp. 73–82, 2015.
- [132] H. Wan, Y. Lu, Y. Xu, and J. Shu, “Empirical study of redo and undo logging in persistent memory,” in *2016 5th Non-Volatile Memory Systems and Applications Symposium (NVMSA)*. IEEE, 2016, pp. 1–6.
- [133] C. Wang, K. He, R. Fan, X. Wang, W. Wang, and Q. Hao, “Cxl over ethernet: A novel fpga-based memory disaggregation design in data centers,” in *2023 IEEE 31st Annual International Symposium on Field-Programmable Custom Computing Machines (FCCM)*. IEEE, 2023, pp. 75–82.
- [134] L. Wang, X. Zhang, S. Wang, Z. Jiang, T. Lu, M. Chen, S. Luo, and K. Huang, “Asynchronous memory access unit: Exploiting massive parallelism for far memory access,” *ACM Transactions on Architecture and Code Optimization*, 2024.
- [135] J. Weiner, N. Agarwal, D. Schatzberg, L. Yang, H. Wang, B. Sanouillet, B. Sharma, T. Heo, M. Jain, C. Tang *et al.*, “Tmo: Transparent memory offloading in datacenters,” in *Proceedings of the 27th ACM International Conference on Architectural Support for Programming Languages and Operating Systems*, 2022, pp. 609–621.
- [136] P. H. Winston, *Artificial intelligence*. Addison-Wesley Longman Publishing Co., Inc., 1992.
- [137] Y. Xu, J. Izraelevitz, and S. Swanson, “Clobber-nvm: log less, re-execute more,” in *Proceedings of the 26th ACM International Conference on Architectural Support for Programming Languages and Operating Systems*, 2021, pp. 346–359.
- [138] J. Yang, J. Kim, M. Hoseinzadeh, J. Izraelevitz, and S. Swanson, “An empirical guide to the behavior and use of scalable persistent memory,” in *FAST*, vol. 20, 2020, pp. 169–182.
- [139] Y. Yang, P. Safayenkoo, J. Ma, T. A. Khan, and A. Quinn, “Cxlmemsim: A pure software simulated cxl. mem for performance characterization,” *arXiv preprint arXiv:2303.06153*, 2023.
- [140] P. Zardoshti, M. Spear, A. Vosoughi, and G. Swart, “Understanding and improving persistent transactions on optane™ dc memory,” in *2020 IEEE International Parallel and Distributed Processing Symposium (IPDPS)*. IEEE, 2020, pp. 348–357.

- [141] J. Zeng, “Compiler and Architecture Co-design for Reliable Computing,” 7 2024. [Online]. Available: https://hammer.purdue.edu/articles/thesis/_b_Compiler_and_Architecture_Co-design_for_Reliable_Computing_b_/26356696
- [142] J. Zeng, J. Choi, X. Fu, A. P. Shreepathi, D. Lee, C. Min, and C. Jung, “Replaycache: Enabling volatile caches for energy harvesting systems,” in *MICRO-54: 54th Annual IEEE/ACM International Symposium on Microarchitecture*, 2021, pp. 170–182.
- [143] J. Zeng, S.-Y. Huang, J. Liu, and C. Jung, “Soft error resilience at near-zero cost,” in *Proceedings of the 38th ACM International Conference on Supercomputing*, 2024, pp. 176–187.
- [144] J. Zeng, J. Jeong, and C. Jung, “Persistent processor architecture,” in *MICRO-56: 56th Annual IEEE/ACM International Symposium on Microarchitecture*, 2023.
- [145] J. Zeng, H. Kim, J. Lee, and C. Jung, “Turnpike: Lightweight soft error resilience for in-order cores,” in *MICRO-54: 54th Annual IEEE/ACM International Symposium on Microarchitecture*, 2021, pp. 654–666.
- [146] J. Zeng, T. Zhang, and C. Jung, “Compiler-directed whole-system persistence,” in *Proceedings of the 51th Annual International Symposium on Computer Architecture*, 2024, pp. 961–977.
- [147] D. Zhang, G. Panwar, J. B. Kotra, N. DeBardeleben, S. Blanchard, and X. Jian, “Quantifying server memory frequency margin and using it to improve performance in hpc systems,” in *2021 ACM/IEEE 48th Annual International Symposium on Computer Architecture (ISCA)*. IEEE, 2021, pp. 748–761.
- [148] H. Zhang, Y. Xue, Y. E. Zhou, S. Li, and J. Huang, “Skybyte: Architecting an efficient memory-semantic cxl-based ssd with os and hardware co-design,” *arXiv preprint arXiv:2501.10682*, 2025.
- [149] X. Zhang, S. Pei, J. Choi, and B. S. Kim, “Excessive ssd-internal parallelism considered harmful,” in *Proceedings of the 15th ACM Workshop on Hot Topics in Storage and File Systems*, 2023, pp. 65–72.
- [150] J. Zhao, S. Li, D. H. Yoon, Y. Xie, and N. P. Jouppi, “Kiln: Closing the performance gap between systems with and without persistence support,” in *Proceedings of the 46th Annual IEEE/ACM International Symposium on Microarchitecture*, 2013, pp. 421–432.
- [151] Y. Zhong, D. S. Berger, C. Waldspurger, R. Wee, I. Agarwal, R. Agarwal, F. Hady, K. Kumar, M. D. Hill, M. Chowdhury, and A. Cidon, “Managing memory tiers with CXL in virtualized environments,” in *18th USENIX Symposium on Operating Systems Design and Implementation (OSDI 24)*. Santa Clara, CA: USENIX Association, Jul. 2024, pp. 37–56. [Online]. Available: <https://www.usenix.org/conference/osdi24/presentation/zhong-yuhong>
- [152] Y. Zhou, J. Zeng, J. Jeong, J. Choi, and C. Jung, “Sweepcache: Intermittence-aware cache on the cheap,” in *MICRO-56: 56th Annual IEEE/ACM International Symposium on Microarchitecture*, 2023.
- [153] Y. Zhou, J. Zeng, and C. Jung, “Lightwsp: Whole-system persistence on the cheap,” in *2024 57th IEEE/ACM International Symposium on Microarchitecture (MICRO)*. IEEE, 2024, pp. 215–230.
- [154] Z. Zhou, Y. Chen, T. Zhang, Y. Wang, R. Shu, S. Xu, P. Cheng, L. Qu, Y. Xiong, J. Zhang, and G. Sun, “NeoMem: Hardware/Software Co-Design for CXL-Native Memory Tiering,” in *2024 57th IEEE/ACM International Symposium on Microarchitecture (MICRO)*. Los Alamitos, CA, USA: IEEE Computer Society, Nov. 2024, pp. 1518–1531. [Online]. Available: <https://doi.ieeecomputersociety.org/10.1109/MICRO61859.2024.00111>
- [155] Q. Zhu, S. Venkataraman, C. Ye, and A. Chandrasekhar, “Package design challenges and optimizations in density efficient (intel® xeon® processor d) soc,” in *2016 IEEE Electrical Design of Advanced Packaging and Systems (EDAPS)*. IEEE, 2016, pp. 47–49.